Received: 29 November 2021 | Revised: 16 December 2021 | Accepted: 30 December 2021

DOI: 10.1002/smm2.1091

REVIEW

SmartMat Open Access WILEY

Vanadium-based metal-organic frameworks and their derivatives for electrochemical energy conversion and storage

Jing Zhu[1] | Xiaoyu Chen[1] | Ai Qin Thang[2] | Fei-Long Li[3] | Dong Chen[4] | Hongbo Geng[3] | Xianhong Rui[4] | Qingyu Yan[2]

[1]Department of Applied Chemistry, State Key Laboratory of Tea Plant Biology and Utilization, Anhui Agricultural University, Anhui, China

[2]School of Materials Science and Engineering, Nanyang Technological University, Singapore, Singapore

[3]School of Materials Engineering, Changshu Institute of Technology, Changshu, Jiangsu, China

[4]School of Materials and Energy, Guangdong University of Technology, Guangzhou, China

Correspondence

Fei-Long Li, School of Materials Engineering, Changshu Institute of Technology, Jiangsu 215500, China.
Email: lifeilong@cslg.cn

Xianhong Rui, School of Materials and Energy, Guangdong University of Technology, Guangzhou 510006, China.
Email: xhrui@gdut.edu.cn

Qingyu Yan, School of Materials Science and Engineering, Nanyang Technological University, Singapore 639798, Singapore.
Email: alexyan@ntu.edu.sg

Funding information

National Research Foundation of Singapore (NRF) Investigatorship, Grant/Award Number: NRF2016NRF-NRFI001-22; National Natural Science Foundation of China, Grant/Award Numbers: 51972067, 22001021, 51802044, 51902062 and 5180204; Guangdong Natural Science Funds for Distinguished Young Scholar, Grant/Award Number: 2019B151502039; Singapore MOE AcRF Tier 1, Grant/Award Number: 2020-T1-001-031; Natural Science Foundation of Jiangsu Province, Grant/Award Number: BK20201048; Natural Science Research

Abstract

With the excessive consumption of nonrenewable resources, the exploration of effective and durable materials is highly sought after in the field of sustainable energy conversion and storage system. In this aspect, metal-organic frameworks (MOFs) are a new class of crystalline porous organic-inorganic hybrid materials. MOFs have recently been gaining traction in energy-related fields. Owing to the coordination flexibility and multiple accessible oxidation states of vanadium ions or clusters, vanadium-MOFs (V-MOFs) possess unique structural characteristics and satisfactory electrochemical properties. Furthermore, V-MOFs-derived materials also exhibit superior electrical conductivity and stability when used as electrocatalysts and electrode materials. This review summarizes the research progress of V-MOFs (inclusive of pristine V-MOFs, V/M-MOFs, and POV-based MOFs) and their derivatives (vanadium oxides, carbon-coated vanadium oxide, vanadium phosphate, vanadate, and other vanadium doped nanomaterials) in electrochemical energy conversion (water splitting, oxygen reduction reaction) and energy storage (supercapacitor, rechargeable battery). Future possibilities and challenges for V-MOFs and their derivatives in terms of design and synthesis are discussed. Lastly, their applications in energy-related fields are also highlighted.

Jing Zhu, and Xiaoyu Chen contributed equally to this study.

Project of Higher Education Institutions in Jiangsu Province, Grant/Award Number: 20KJB150008

KEYWORDS
derivatives, electrocatalysis, rechargeable battery, supercapacitor, V-based metal-organic frameworks

1 | INTRODUCTION

Over the last few decades, tremendous efforts have been devoted to exploring advanced electrochemical energy conversion and storage systems due to the rapid exhaustion of fossil fuels and the deterioration of global warming.[1–3] Electrochemical energy conversion systems have been proven as one of the cleanest and most sustainable ways to alleviate energy and environmental problems. Water splitting, fuel cells, metal-air batteries (MABs), and carbon/nitrogen fixation have shown effectiveness in the production and utilization of electrofuels (e.g., H_2 or CO), as well as in the treatment of greenhouse gases (CO_2).[4–9] Electrocatalysis through the hydrogen evolution reaction (HER), oxygen evolution reaction (OER), and oxygen reduction reaction (ORR) are indispensable routes for most of the energy conversion devices.[10–13] However, the respective electrocatalysts consume tremendous amount of electrical energy due to the large overpotential and slow kinetics. In addition, the catalysts are expensive and have relatively short lifespans. These shortcomings hamper the possibility for large-scale applications in commercial equipment which are typically subjected to harsh conditions.[14,15] On the other hand, supercapacitors (SCs), metal (lithium, sodium, and potassium) ion batteries, and lithium-sulfur batteries (LSBs) are promising electrochemical energy storage devices for portable electronics and electric vehicles.[16–18] Nevertheless, these energy storage devices are still limited by their inherent safety issues. These devices face uncontrolled growth of metal dendrites, serious shuttle effects, and drastic change in the volume of the electrode material which adversely affect the rate capability, cycle life, and security. Further rectifications are required to meet the multifaceted demands from the market.[19,20] In view of the above-mentioned issues, the development for more efficient yet durable electrocatalysts and electrode materials with desirable electrochemical properties are of the utmost importance. Carbon-based materials,[21–26] gel-based materials,[27] Prussian blue analogues (PBAs)-based materials,[28] conducting-polymer-based materials,[29] transition metal dichalcogenide-based materials,[30–32] perovskite-type oxides,[33] metal sulfides,[34] layered double hydroxides (LDHs),[35] MXenes[36–40] are some of the materials that were investigated recently by researchers in hopes to meet the demands.

Apart from those, metal-organic frameworks (MOFs) are part of emerging porous crystalline materials that are being intensely researched in the past two decades, particularly in terms of design synthesis and modification.[41–45] MOFs are a class of organic-inorganic hybrid materials, consisting of metal nodes (ions or clusters) and various organic ligands, and they provides promising potential to be used in selective gas adsorption and separation, hydrogen storage, chemical sensors, heterogeneous catalysis, and drug delivery.[46–53] Research has also shown that MOFs with abundant metal sites, porous structures, and lager specific surface areas can offer more accessible active sites and faster mass/charge transfer, thus improving the electrochemical performance of electrocatalysts and electrode materials.[54–57] The pristine and modified forms can provide various functionalities and benefits in different applications. While MOFs composites are assembled with functional species, including graphene, carbon nanotubes (CNTs), metal nanoparticles, MXenes, covalent-organic frameworks (COFs), and even enzymes,[58,59] which exhibit synergistic effects and multifunctionality. Besides, MOFs derivatives provide high conductivity and robust structure.[60–64] The types of MOFs are manifold. This review will provide an overview of the rarely reported MOFs.

In comparison to MOFs based on divalent metals (Zn^{2+}, Ni^{2+}, Cu^{2+}, etc.) coordination nodes, MOFs based on trivalent or tetravalent metals are rarely reported due to the complexity of their node clusters and the flexibilities of their coordination environments. Vanadium (V), a common transition metal, belongs to the fifth subgroup with $3d^34s^2$ on its outer electron layer structure. This means that it has abundant valence electrons to allow a variety of redox behaviors.[65–67] Thus, V-based materials (vanadium oxide, vanadium nitride, vanadium sulfide, mixed metal vanadate, vanadyl phosphate) may be applied for future development of electrochemical energy conversion and storage technologies.[68–73] V-based MOFs (V-MOFs), specifically on those with V ions or clusters occupied in the vertex positions of its polyhedral structure, have recently gained traction due to their multiple valence states and open-framework crystal structure. These could then lead to high specific capacity, remarkable cycle stability, and considerable electrocatalytic performance.[74] Moreover, it is very encouraging that MOFs as precursors can not only provide new synthetic ideas for the design of V-based materials, but also endow them with unique structure, high specific surface area, excellent

conductivity, and robust stability. These will then promote the rapid diffusion of electrolyte and improve electrochemical performance significantly.[75]

The application of V-MOFs in energy-related fields has not yet been reviewed widely. This review will cover the applications, its recent advances, and challenges of using V-MOFs and their derivatives as electrocatalysts or electrode materials. This review will discuss the various kinds of V-MOFs and their derived materials that have been reported, followed by their present applications in electrochemical energy conversion (HER, OER, ORR) and storage (SCs, metal ion batteries) (Scheme 1). Finally, the future direction and challenges for the development of V-MOFs and their derivatives in terms of energy-related applications will be discussed.

2 | V-MOFS

The formation of V-MOFs is usually a process of self-assembly of vanadium ions and organic ligands to form a network structure. As an essential metal unit, vanadium trichloride (VCl_3), vanadyl sulfate ($VOSO_4$), and vanadium powder are often used as vanadium sources, which are usually connected with each other by the polytopic carboxylate linkers or nitrogen-containing heterocycles to form three dimensional frameworks with different topologies. The typical synthetic strategies, include hydro/solvothermal method, ultrasonic method, and coprecipitation method, provide layouts to design and prepare different morphologies of V-MOFs.[76–78] According to the composition and form of vanadium nodes, V-MOFs in this review are deliberately divided into three parts: (1) the pristine V-MOFs, (2) mixed-metal MOFs (V/M-MOFs, M refers to other metal nodes), and (3) polyoxovanadate-based MOFs (POV-MOFs).

2.1 | The pristine V-MOFs

Although tremendous efforts have been made to synthesize crystalline V-MOFs, only a few crystalline V-MOFs, such as MIL-47,[79] MIL-68[80] and MIL-59[81] (MIL stands for Materials of Institute Lavoisier), can be accurately determined by single-crystal X-ray diffraction (SXRD) based on their crystal structures. To overcome such ordeal, crystallographers can use either synchrotron radiation or powder X-ray diffraction (PXRD) to create desired MOFs structures for various applications. This results in having a wide variety of V-MOFs being reported in recent years (Figure 1).[78–89]

The two widely known structural motifs of building units for the connection form of V containing nodes are

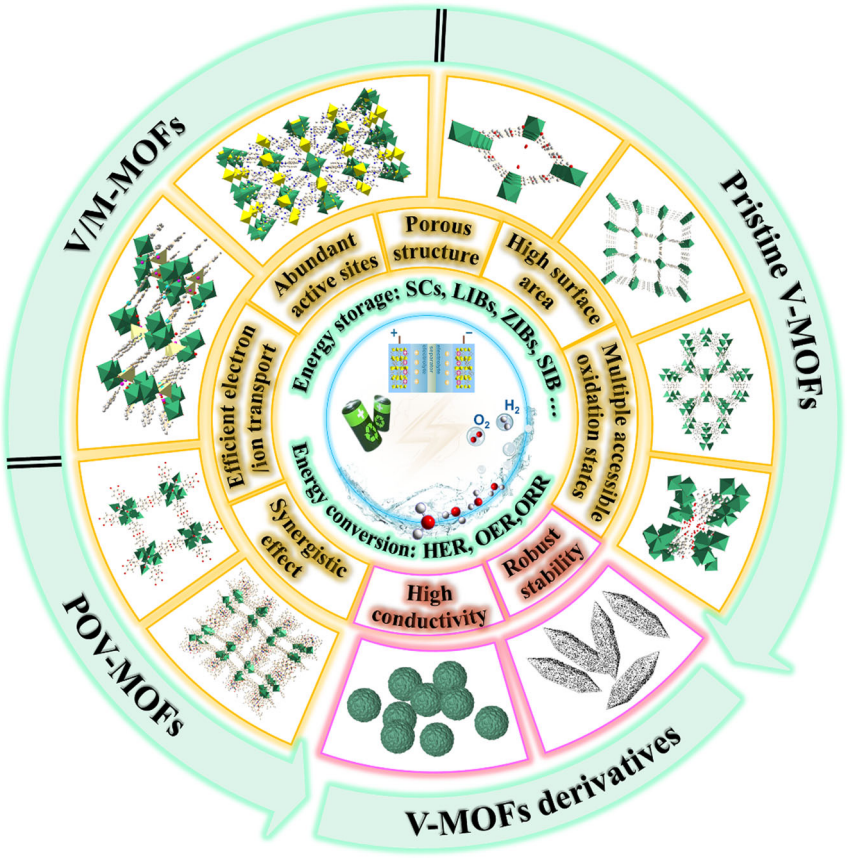

SCHEME 1 An overview of V-MOFs and their derivatives used in energy conversion and storage. V-MOF, vanadium-metal-organic frameworks

infinite trans chains of $[V^{III}(OH)_2O_4]$ octahedra, and oxo-centered trimers of vanadium octahedra (Figure 1). In the case of the former, the synthetic form of V-MOFs contains octahedral $[V^{III}(OH)(R\text{-}(CO_2)_2)]$ infinite long chains, and some of the representatives include MIL-47,[79] MIL-68,[80] COMOC-2,[78] COMOC-3,[82,88] (COMOC stands for Center for Ordered Materials, Organometallics and Catalysis, Ghent University) MIL-60,[83] and MIL-71.[84] Among them, MIL-47 has been widely studied because of its large pores (aperture sizes: 10.5×11.0 Å, taking into account the van der Waals radii), flexible and open structure, as well as the large specific surface area ($S_{BET} = 930\ m^2/g$, $S_{Langmuir} = 1320\ m^2/g$).[90–100] From a structural point of view, it is built from infinite chains of corner-sharing VO_6 octahedra and interconnected by terephthalate groups, creating a three-dimensional topology of orthorhombic structure. MIL-47 also exhibits the similar breathing effects to MIL-53 (Cr),[101,102] the guest molecules trapped in V-MOFs possessing $\{V-O-V\}_\infty$ chains which can be removed by thermal activation to form empty pores. The cell volume will then increase by 40%, converting itself from the narrow pore form (NP) to the large pore form (LP). In addition, the $V^{III}-OH$ bond can be oxidized to the vanadium-oxygen double bond, increasing the valence state of vanadium from +3 to +4, without affecting its original topological

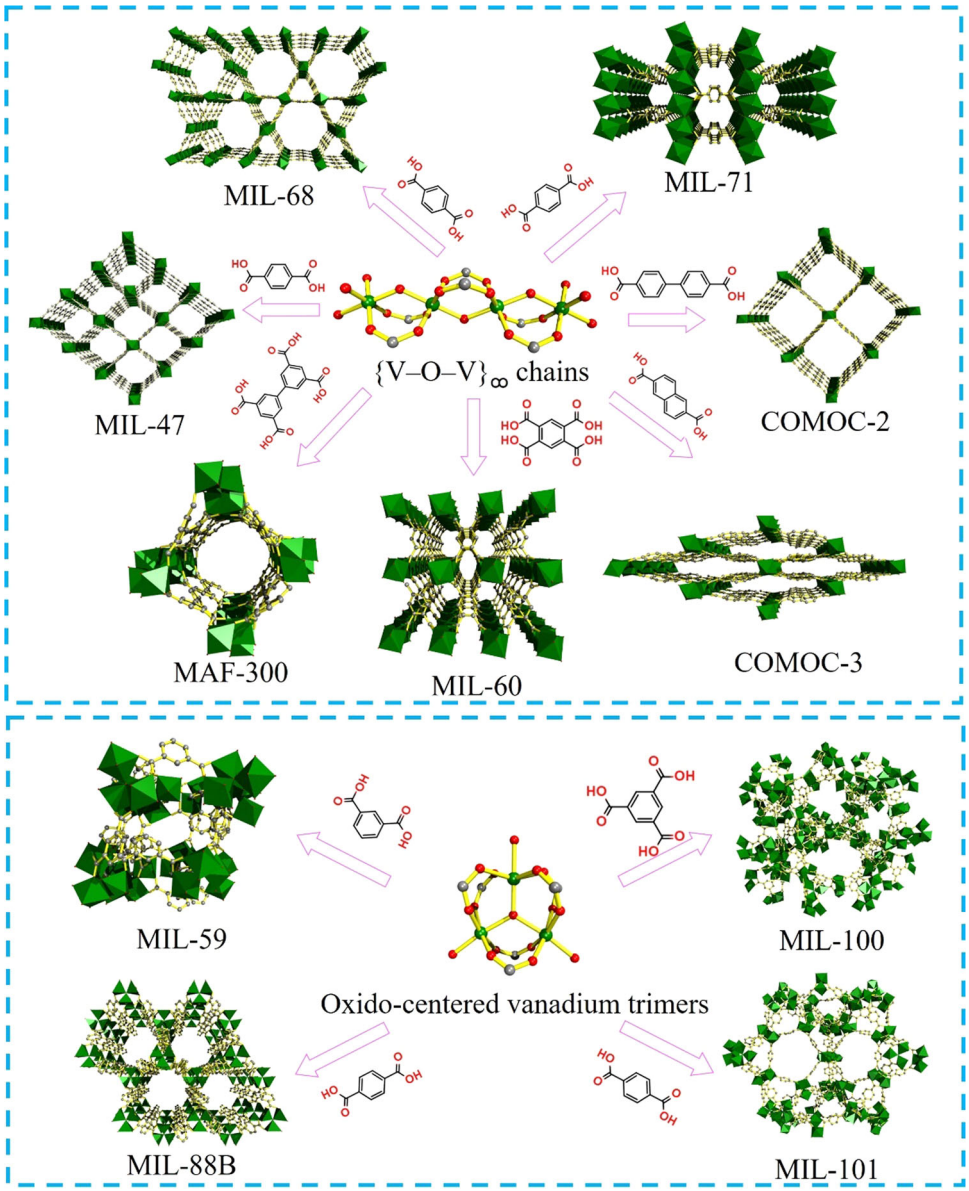

FIGURE 1 Crystal structures of representative V-MOFs. COMOC-2,[78] MIL-47,[79] MIL-68,[80] MIL-59,[81] COMOC-3,[82] MIL-60,[83] MIL-71,[84] MFM-300,[85] MIL-88B,[86] MIL-100[88] and MIL-101.[87] Color codes: V, green; C, grey; O, red

structure.[79] On the other hand, some V-MOFs (MIL-59,[81] MIL-88B,[86] MIL-100,[88] and MIL-101[87]) possessing the general formula $[V_3O(OOCR)_6L_3]^{n+}$ (L = terminal ligand: H_2O or Cl^-) contain oxo-centered vanadium trimers in the framework structure. As shown in the crystal structure of MIL-100 and MIL-101 in Figure 1, the trimers are interlinked by polycarboxylates to form the supertetrahedra (ST), which are further interconnected in three-dimensional (3D) fashion to produce the augmented zeolite mobil thirty-nine (MTN) type of framework. Therefore, both MIL-100 and MIL-101 networks exhibit cage-like structures, which is suitable as host materials for energy storage.[87,89]

In addition to the structural differences caused by the secondary building units (SBUs), the design and modification of ligands also play important roles in the structural characteristics and functionality of V-MOFs. It is well known that the properties (pore size or chemistry) of a particular MOF can be systematically adjusted without changing the basic topological structure. This can be done by introducing functional groups (with different sizes, polarity, acidity, etc.) in the organic linkers. Vanpoucke et al.[90] investigated the effect of ligand functionalization to regulate the electronic structure of V-MOFs, revealing that the introduction of functional groups brought about a splitting of the π orbital on the chain due to their electron-withdrawing/donating nature. The organic ligands modified by diverse functional groups ($X = -Cl$, $-Br$, $-CH_3$, $-CF_3$, $-OH$, $-OCH_3$, etc.) can also be used as a linker to synthesize a series of V-MOFs whilst maintaining their phase purity.[103–105] Additionally, Yot et al.[97] reported that the large molecular weight functional groups ($-Br$ or $-CF_3$) functionalized ligands can also improve the mechanical energy storage performances of these hybrid porous materials. In comparison with MIL-101 (V), the amino-modified MIL-101 (NH_2-MIL-101) do not only have a larger specific surface area, but also demonstrate higher CO_2/N_2 adsorption capacity and moderate CO_2 isosteric heat of adsorption.[106] Moreover, the steric resistance and physical property of the substituent for the ligands also have certain influence on the construction of MOFs.

In general, the abundant coordination environment of V ions enables the structural diversity of the pristine V-MOFs, where the porous character and coordinatively unsaturated metal sites offer the possibility of energy storage and conversion. And the control of the ligands also facilitates the modulation of the electronic structure of the electrocatalytic active site. In addition, it is worth looking forward to the richness of the pristine V-MOFs to offer more options for the design and synthesis of V/M-MOFs and V-MOFs derivatives.

2.2 | V/M-MOFs

With the help of the modular building principle, different metal ions with similar structural roles in the construction of MOFs can be intentionally integrated into molecular scaffolds to produce mixed-metal MOFs.[107,108] The mixed metal nodes can self-assemble in an equivalent manner and occupy random positions in its final MOF skeleton. It is well known that MIL-53 (M) (M = Al, Fe, Cr, etc.) is a general term for a class of well-known homologous carboxylate-based MOFs, consisting of an infinite chains of corner-sharing $MO_4(OH)_2$ octahedra.[109,110] As an analogue of MIL-53, V-MOFs ($[V^{III}(OH)bdc]_n$) features a similar crystal structure. Therefore, a series of mixed-metal V/M-MOFs (M = Al,[111] Ni,[112] Fe,[113]) have been prepared by direct synthesis, obtaining same phase as MIL-53. Significantly, "V-doping" has a positive impact on the adsorption and electrocatalytic properties of MOFs materials due to the possible stabilization of the mixed-valence V^{III}/V^{IV} oxidation states in its pure activated phase. Also, based on the modular principle, Rocha et al.[114] reported the construction of a series of modular trinodal mixed-metal V/La-MOFs via self-assembly of V-containing cyclic trinuclear anionic units with cationic $\{MO_8\}$ or $\{MO_9\}$ aqua-based lanthanide complexes. Unlike the relatively independent secondary building units, the heterobimetallic SBUs connect two different metal centers by a short bridge and have great potential for the construction of metal-organic polymers.[115] Senchyk et al.[116] successfully integrated the novel Ag^I/VOF (VOF stands for vanadium oxofluoride) heterobimetallic complexes into MOFs employing 1,2,4-triazole ligands with aliphatic linkers, whereby a series of novel Ag^I/V^V-MOFs were successfully synthesized by a simple one-pot hydrothermal methodology (Figure 2A).

Moreover, the post-modification strategy has also been proven to be an effective method for the synthesis of V/M-MOFs. MFU-4*l* ($[Zn_5Cl_4(BTDD)_3]$, BTDD: bis(1H-1,2,3-triazolo[4,5-b],[4′,5′-i])dibenzo[1,4]dioxin) (MFU stands for Metal-organic Framework Ulm-University) can be modified post-synthetically via partial or complete substitution of peripheral metal sites, thus opening a route towards a large variety of functionalized MOFs.[120–122] Comito et al.[117] reported the incorporation of vanadium into MFU-4*l* by cation exchange to prepare two benzotriazolate-based V/Zn-MOFs, and vanadium incorporation can be observed when each of the precursors was used in a modest excess (Figure 2B). When VCl_4 or $VCl_3(THF)_3$ (THF: tetrahydrofuran) was used as a precursor, the as-prepared V^{IV}/Zn-MOFs showed nearly identical edge energies and pre-edge features. By contrast, MFU-4*l* exchanged with $VCl_2(py)_4$ (py: pyridine) exhibited an edge energy most consistent with vanadium (II).

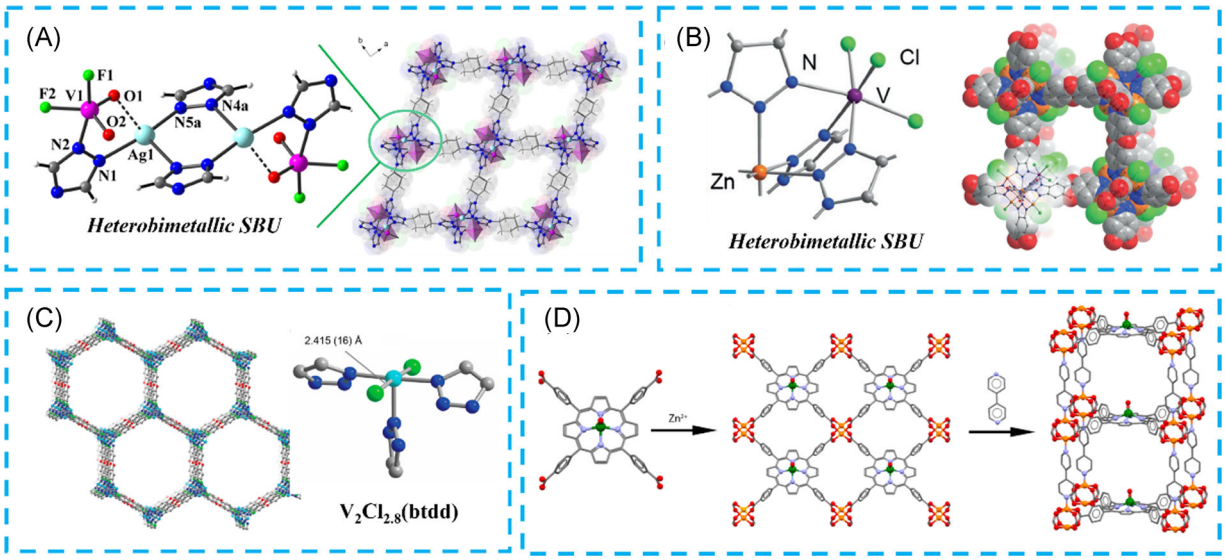

FIGURE 2 (A) Ag/VOF building fragment as a node of the "square grid" framework topology with linear triazolyl linkers in the crystal structure. Reproduced with permission: Copyright 2012, American Chemical Society.[116] (B) The structure of V^{IV}-MFU-4*l*. Reproduced with permission: Copyright 2018, Wiley-VCH.[117] (C) The structure of $V_2Cl_{2.8}$(btdd) and primary V^{II} coordination sphere. Cyan, green, blue, red, and grey spheres represent V, Cl, N, O, and C, atoms, respectively. Reproduced with permission: Copyright 2021, American Chemical Society.[118] (D) Schematic illustration of a two-step self-assembly process that is responsible for the formation of the VO(TCPP-Zn_2-bpy). Color codes: green, V; orange, Zn; red, O; light blue, N; gray, C. Reproduced with permission: Copyright 2018, American Chemical Society[119]

The same ligand can also be used to synthesize monometallic MOF ($V_2Cl_{2.8}$(btdd)), with a structure containing one-dimensional hexagonal channels and vertices that are decorated by vanadium sites. It is worth noting that $V_2Cl_{2.8}$(btdd) is a mixed-valent, containing 40% V^{III} sites, charge-balanced by terminal chloride ligands, and 60% V^{II} sites in a square pyramidal geometry (Figure 2C).[118,123]

The heterometallic MOFs can also be synthesized from metalloligands such as pyridine-2-carboxylates,[124] Schiff bases,[125,126] metallosalen,[127,128] and other ligands.[129,130] On the other hand, porphyrins are different from other metalloligands. The cavity inside porphyrins can adopt numerous metal elements, and the 3D stacking of porphyrin-based MOFs can be controlled by the coordination geometry of the porphyrin metal center to form the well-known porphyrin paddle-wheel frameworks (PPFs).[131] When choosing different types of metalloporphyrin and paddle-wheel clusters, various frameworks with the same topology can be obtained, while the pore size can be controlled by changing the columnar molecules that connect the two porphyrin layers. Besides, due to the presence of porphyrins, PPFs are expected to have a unique feature: possessing a large number of coordination unsaturated metal centers, which plays a key role in applications such as gas adsorption and catalytic conversion.[132] Yamabayashi et al.[119] have successfully synthesized a 3D porous vanadyl-based MOF, [VO(TCPP-Zn_2-bpy)] (TCPP: tetracarboxylphenylporphyrinate; bpy: 4,4′-bipyridyl), and investigated how such structural modifications influence qubits' performances. Similar to [Cu(TCPP)-$Zn_2(H_2O)_2$] reported by Urtizberea et al.,[133] the peripheral carboxyl substituents of the metalloporphyrin macrocycle interacted with Zn^{2+} to form two-dimensional (2D) layers, and then the pillar-like bpy ligands allow connection between the 2D layers to form a 3D MOF by further axial coordination between pairs of [$Zn_2(COO)_4$] subunits. The result shows that the introduction of vanadyl units in the 3D network has an obvious effect on the infrared-active low-energy vibrational modes (Figure 2D). In contrast, research on similar 2D planes without pillars are relatively scarce, Urtizberea et al.[103] have also successfully synthesized 2D-MOF [{VO(TCPP)}$Zn_2(H_2O)_2]_\infty$ at the air-water interface, even allowing mono- and multiple-layer deposits to be transferred to various substrates. Compared with the pristine V-MOFs, V/M-MOFs have obvious regulatory advantages in terms of structure and composition, which provide more active sites for electrocatalytic applications. Besides, V/M-MOFs also enrich the kinds of precursors and the corresponding derivatives.

2.3 | POV-MOFs

Polyoxometalates (POMs) composed of transition metals (mainly vanadium, molybdenum, tungsten) and oxide cluster with high negative charge.[134] POMs have discrete

anionic oxidation-bridged metal clusters, which have been widely studied in the field of energy materials research recently due to their stable structures and remarkable catalytic activities.[135] Addition of POMs into various pore supports, such as mesoporous silica,[136] and molecular sieves[137] is a commonly adopted strategy to enhance the stability and reusability of POMs. Alternatively, POM anions can also be used as inorganic units to construct a variety of POM-based MOFs.[138–140] As an important subclass of POMs, polyoxovanadates (POVs) have abundant redox behaviors due to the multiple accessible oxidation states (mainly based on the V^{V}/V^{IV} and more rarely V^{IV}/V^{III} redox couples). With that, POV-MOFs have gained traction because of their unique structures and electrochemical performances.[141]

A cubane (V_4O_{16})-based MOFs expressed as $Cu_2(phen)_2(V_4O_8)(PO_4)_4$ [$Cu_2V_4O_{16}$-2D] (phen: phenanthroline) for transition metal (Cu^{II}) connections were reported for the first time by Dey et al.[142] The bulk material exhibited two different morphologies, but both possessed the same structure (Figure 3A). From the perspective of the structure, four edge-sharing VO_6 octahedra were packed together to form one V_4O_8 cubane unit, and each V_4O_8 cubane was connected to four different Cu(phen)$(O)_3$ square pyramidal units (Figure 3B). Similarly, other clusters such as Wells-Dawson-type tungstovanadate clusters ($[V_2W_{18}O_{62}]^{6-}$) were also used to construct POV-MOFs with 3D self-penetrated frameworks.[145] Liu's research team[143] has also made tremendous contribution in the design and synthesis of POV-MOFs in recent years. Two novel POV-MOFs, [Co(bib)]$\{V_2O_6\}$ (V-Co-MOF) and [Ni(en)(bib)]$\{V_2O_6\}\cdot 2H_2O$ (V-Ni-MOF) (bib: 1,4-bis(1H-imidazoly-1-yl)benzene; en: ethylenediamine) were synthesized under mild hydrothermal conditions, and V sites with both of them adopted the $\{VO_4\}$ tetrahedral coordination geometry.

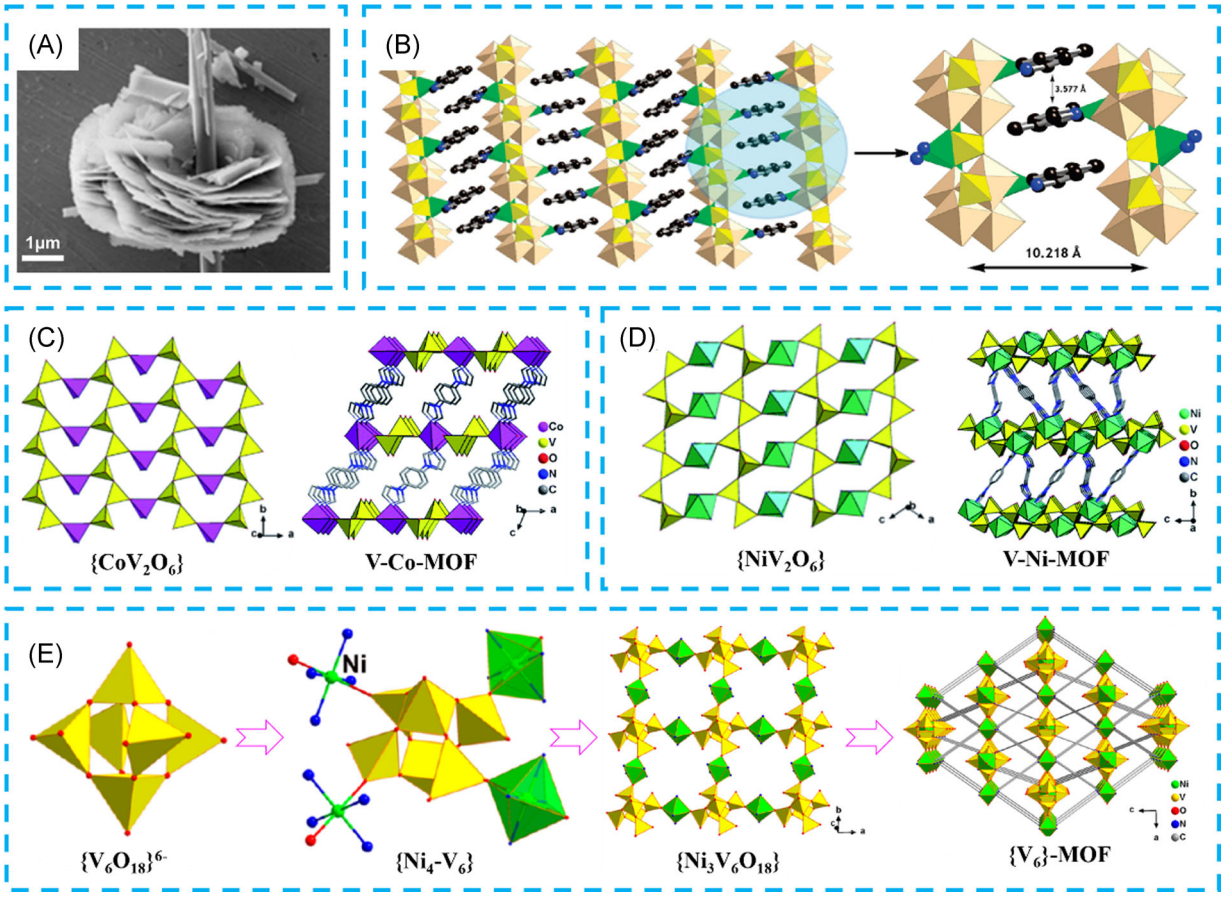

FIGURE 3 (A) SEM image of the bulk $Cu_2V_4O_{16}$-2D. (B) Interdigitation of 2D sheets of $Cu_2V_4O_{16}$-2D via the phenanthroline ring in the ac-plane. Color code: black, C; green, Cu; red, O; blue, N; yellow, P; dark yellow, V. Reproduced with permission: Copyright 2011, American Chemical Society.[142] (C) The 2D bimetallic oxide layers and 3D frameworks of the V-Co-MOF. (D) The 2D bimetallic oxide layers and 3D frameworks of the V-Ni-MOF. Reproduced with permission: Copyright 2020, Royal Society of Chemistry.[143] (E) A schematic illustration of the crystal structures of {V6}-MOF: $\{V_6O_{18}\}^{6-}$ polyanion cluster, bimetallic decanuclear cluster $\{Ni_4\text{-}V_6\}$, 2D bimetallic oxide layer $\{Ni_3V_6O_{18}\}$ and 3D framework of $\{V_6\}$-MOF. Reproduced with permission: Copyright 2021, American Chemical Society.[144] 2D, two-dimensional; 3D, three-dimensional; MOF, metal-organic framework; SEM, scanning electron microscopy

It is worth noting that the Co centers in V-Co-MOF exhibited tetra-coordination twisted in tetrahedral configuration (coordination unsaturated metal sites, CUMS) (Figure 3C), and the Ni centers in V-Ni-MOF showed hexa-coordination octahedral geometry (coordination saturated metal sites, CSMS) (Figure 3D).[143] Under the same conditions, the catalytic performance of V-Co-MOFs was better than that of V-Ni-MOFs due to the synergistic effect of V^V sites and Co^{II} centers. Furthermore, $[Ni(Bib)_2]\{V_2O_6\}$ ($\{V_6\}$-MOF) can also be synthesized by hydrothermal method.[144] Unlike the above two POV-MOFs containing 1D $\{V_2O_6\}^{2-}$ polyanion chains, the $\{V_6\}$-MOF contained a hexa-nuclear vanadium anion cluster ($\{V_6O_{18}\}^{6-}$), which only composed of two VO_5 tetragonal pyramids and four VO_4 tetrahedrons, connected by the apex sharing of O atoms (Figure 3E). Different from the pristine V-MOFs and V/M-MOFs materials, the most distinctive feature of POV-MOFs is that their building unit nodes are POVs rather than simple metal ions. And excellent stability, diverse valence states and rich composition of POVs can improve the catalytic activity and stability of V-MOFs, thus broadening their applications in electrochemistry.

3 | DERIVATIVES OF V-MOFS

When V-MOFs were used as precursors or templates, various forms of derivatives can be obtained, such as vanadium oxide, carbon-coated vanadium oxide, vanadium phosphate, vanadate and other vanadium doped nanomaterials (Figure 4).[146–154] The transformation pathway and theory of V-MOFs to related V-MOFs derived carbon, metal compounds and their composites are relatively complex. This is because they are drastically affected by the composition and structure characteristics of their precursors, pyrolysis temperature, calcination atmosphere and other transformation conditions.[155] Taking the calcination atmosphere as example, the heat treatment process can be divided into two cases: in air and in inert atmosphere. When annealed in air, organic components volatilize into CO_2 or retain a small amount of porous carbon, while vanadium metal units are being oxidized to form a variety of vanadium oxides with nanostructures. In addition, V-MOFs precursors also have a significant effect on the morphology and composition of their derivatives. On the one hand, the organic ligands are in-situ carbonized in the inert atmosphere to produce porous carbons with high specific surface areas, thus improving the stability and electrical conductivity of electrocatalysts or electrode materials. On the other hand, the V-MOFs derivatives usually retain the specific morphology of the precursors and provide highly tunable feature of spatial distribution of derived nanostructures, where the distribution of metal components and carbon is homogeneous, which is difficult to achieve with mixed carbon alone. More interestingly, due to the different mobilities of the atoms in the precursors of V-MOFs, derivatives with novel hollow structures can also be formed by the Kirkendall effect. Furthermore, the corresponding vanadium-based sulfides, selenides and phosphating materials can also be synthesized by annealing in the presence of sulfur, selenium, or sodium hypophosphite.

During the pyrolysis process, most V-MOFs derivatives can maintain the original skeleton structure and morphology of V-MOF at low temperature (<600 °C), while endowing materials with controllable pore size and new morphology such as multi-layer core-shell structure.[146,149] For example, vanadium phosphate with multi-layer core-shell, nanosheet and nanowire can be prepared by ion exchange.[150] The composition and crystal phase of these derived materials, as well as the abundance of active metal sites and unsaturated organic sites do not only expand the electrochemical active surface area, but also increase the effective electron transport. In view of energy conversion and storage, V-MOFs can be directly used as electrocatalysts and electrode materials, or as sacrificial templates to prepare porous carbon matrix supported metal compounds to obtain various nanostructures and higher electrochemical performances. The following two sections will discuss the application of V-MOFs and derivatives in electrochemical energy conversion and energy storage.

4 | ELECTROCHEMICAL ENERGY CONVERSION

Electrochemical energy conversion technology adopts clean process and has little impact on the environment, which plays a very important role in the sustainable development of energy.[156,157] Electrochemical water splitting is considered as one of the most promising energy conversion technologies for hydrogen production from water, which consists of two half reactions: OER at the anode and HER at the cathode.[158,159] Proton exchange membrane fuel cell (PEMFC), as an efficient alternative energy conversion device for direct chemical-to-electrical energy conversion, has also attracted widespread attention, among them, cathodic ORR is a multi-electron, multi-step reaction with sluggish kinetics, which then deemed as the critical limiting step, and consumed most catalyst materials.[160,161] Efficient electrocatalysts are prepared for these electrochemical reactions to reduce their overpotentials for practical applications, and

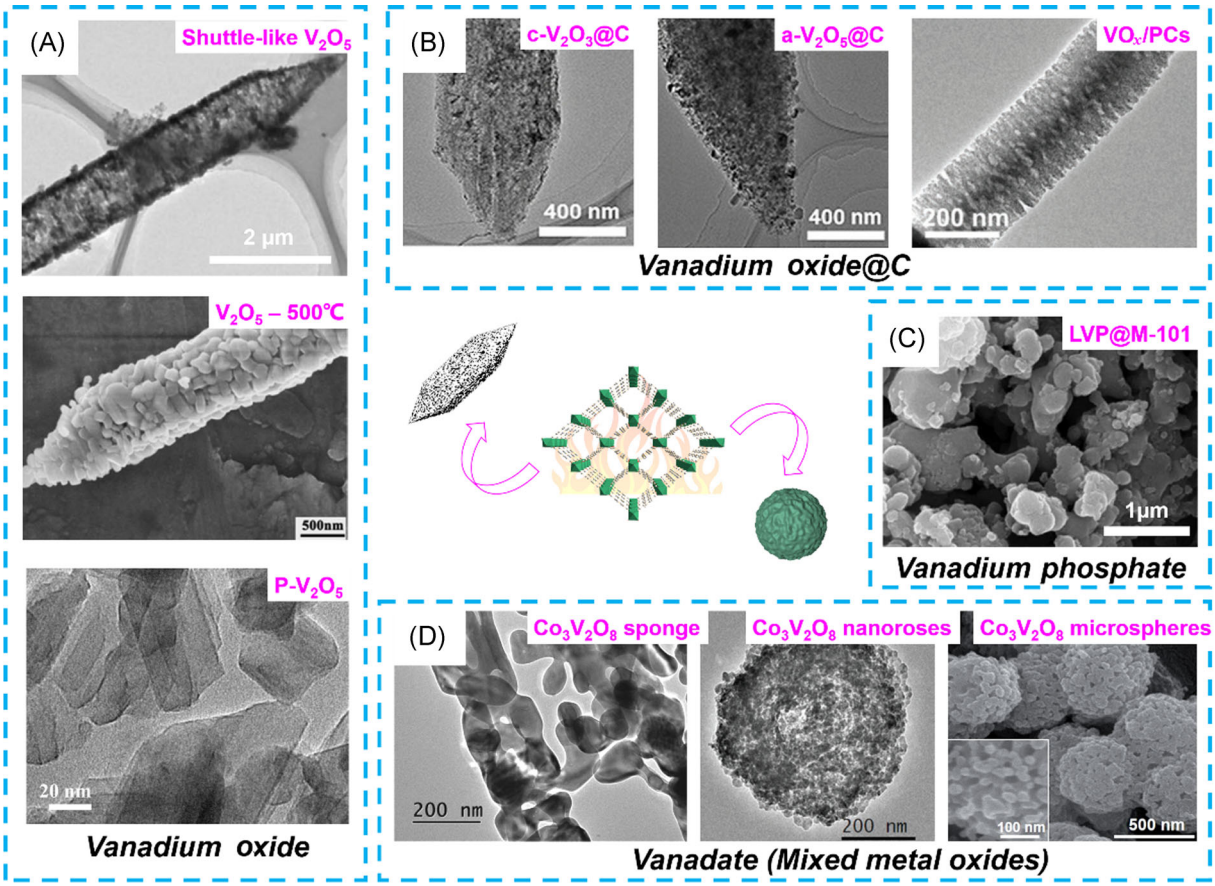

FIGURE 4 An illustration of the transformation of V-MOF to derivatives, and the electron microscopic images of some V-MOFs derivatives, including: (A) Vanadium oxide: shuttle-like V_2O_5, Reproduced with permission: Copyright 2017, Springer Nature Limited[146]; V_2O_5-500 °C, Reproduced with permission: Copyright 2020, Springer Nature Limited[147]; P-V_2O_5 (porous V_2O_5), Reproduced with permission: Copyright 2019, Elsevier B.V.[148] (B) Vanadium oxide@C: c-V_2O_3@C (crystalline V_2O_3 and carbon composite), a-V_2O_5@C (amorphous V_2O_5 and carbon composite), Reproduced with permission: Copyright 2020, Wiley-VCH[149]; VO_X/PCs, Reproduced with permission: Copyright 2018, Wiley-VCH.[150] (C) LVP@M-101 (carbon-coated $Li_3V_2(PO_4)_3$ nanocomposites), Reproduced with permission: Copyright 2018, Elsevier B.V.[151] (D) $Co_3V_2O_8$ sponge, Reproduced with permission: Copyright 2016, American Chemical Society[152]; $Co_3V_2O_8$ nanoroses, Reproduced with permission: Copyright 2017, Royal Society of Chemistry[153]; $Co_3V_2O_8$ microspheres, Reproduced with permission: Copyright 2016, Royal Society of Chemistry[154]

a variety of V-MOFs and derivatives for electrocatalysis have been summarized in Table 1.

4.1 | V-MOFs as electrocatalysts

The homogenous dispersed metal ions (or clusters), along with the ultrahigh specific surface area of MOFs enable electrocatalysts to provide abundant active sites for water splitting. Furthermore, the poor electronic conductivity of MOFs can be improved to some extent by using nickel foam[167] or other carbon nanoparticles[168] as substrates. It is well known that most bimetallic and polymetallic-based electrocatalysts demonstrate significantly better performance than their monometallic-based counterparts, because the electronic configuration of monometallic electrocatalysts can be adjusted by introducing other metals, yielding significant improvement in their catalytic activities.[169] Taking advantage of the synergistic effect of multiple metals, some V/M-MOFs electrocatalysts have been developed for water splitting, where the M ions usually act as the active center of the electrocatalysis, and V ions with abundant oxidation states often play the role of regulating the electronic structure of the active sites.

Using nickel and vanadium as raw materials, the three-dimensional nickel-vanadium-based MOFs supported on nickel foam (Ni_2V-MOFs@NF) was synthesized by two-step of method: ultrasonic and hydrothermal at the ratio of 1:2 (Figure 5A).[112] Ni_2V-MOFs@NF attained the current density of 10 mA/cm^2 (η_{10}) at very low overpotentials of 244 and 89 mV with the low Tafel slopes of 38.1 and 98.3 mV/dec for OER and HER, respectively. Furthermore, this

TABLE 1 Comparison of the performance of V-MOFs and their derivatives for electrocatalysis

Electrocatalysts	Electro-catalytic reactions	Electrolyte	Current density (mA/cm^2)	Overpotential (mA)	Tafel slopes (mV/dec)	Refs.
V-MOFs:						
Ni_2V-MOFs@ NF	HER	1 mol/L KOH	10	89	98.3	[112]
	OER	1 mol/L KOH	10	244	38.1	
V/Fe-MOF@ NF	HER	1 mol/L KOH	10	147	208.3	[113]
	OER	1 mol/L KOH	10	246	42.6	
$[Ni_2(BBTZ)(H_2O)_4]$ $V_4O_{12}\cdot 2H_2O$	OER	1 mol/L KOH	10	353	77.8	[162]
V-MOFs derivatives:						
MOF-V-Ni_3S_2/NF	HER	1 mol/L KOH	10	118.1	113.2	[163]
	OER	1 mol/L KOH	10	268	99	
CoVO/C	OER	1 mol/L KOH	10	350	75	[164]
V-Co_xP@NC	HER	1 mol/L KOH	10	106	93	[165]
	OER	1 mol/L KOH	50	354	79	
V-Ni_xFe_y-MOF@GO	HER	0.5 mol/L H_2SO_4	10	90	150	[166]
	OER	1 mol/L KOH	10	210	97	

Abbreviations: HER, hydrogen evolution reaction; OER, oxygen evolution reaction; V-MoF, vanadium metal-organic framework.

bifunctional electrocatalyst can also realize a cell voltage of 1.55 V at a current density of 10 mA/cm^2, which is comparable to the commercial electrocatalysis (Figure 5B). In addition, the chronopotentiometry also proves that the electrolytic cell for water electrolysis had excellent stability (Figure 5C). The superior performance of these new synthetic electrocatalysts would give the credit to the special morphology from the 2D ultrathin nanosheets self-assembling to a 3D nanoflower, as well as the electronic properties manipulation caused by the synergetic effect between Ni ions and V ions. Additionally, the incorporation of high-valent vanadium reduces the band gap of Ni_2V-MOFs and improves the electron conductivity. With the same strategy of morphological control and electronic regulation, Han et al.[113] reported the preparation of well-defined arrays of V/Fe-MOF with controllable stoichiometry supported on NF through the ultrasound and solvothermal synthesis method (Figure 5D). Notably, V-MOF@NF and Fe-MOF@NF obtained by the same synthesis method depict different microscopic characteristics, and only the former can form array structure. This proves that the presence of V element played an important role in the formation of array. For the combination of V^{2+} and Fe^{2+} in bimetallic V/Fe-MOF@NF, the π-bond of Fe −O would increase due to the repulsion between O^{2-} and V^{2+}, thus resulting in a portion charge transfer from V^{2+} to Fe^{2+} (Figure 5E). The morphological control and electronic regulation strategy for the synthesis of V/Fe-MOF@NF has led to a high electrocatalytic activity in alkaline electrolyte with a relatively low overpotential of 246 mV@10 mA/cm^2 for OER and 147 mV@10 mA/cm^2 for HER, respectively. V/Fe-MOF@NF can also provide a current density of 10 mA/cm^2 at a low cell voltage of 1.61 V, which was better than the single metal MOF catalysts (V-MOF@NF and Fe-MOF@NF) (Figure 5F). There was no obvious degradation for the current density after 3600 s of continuous water-splitting reaction, indicating the remarkable high electrochemical stability of the V/Fe-MOF@NF | | V/Fe-MOF@NF couple (Figure 5G).

Hu et al.[162] also investigated the role of POVs in electrocatalytic water oxidation reaction. Three bulk POV-MOFs materials, $[Ni_2(BBTZ)(H_2O)_4]V_4O_{12}\cdot 2H_2O$ (1), $[Co_2(BBTZ)(H_2O)_4]V_4O_{12}\cdot 2H_2O$ (2), $[Ni(BBTZ)_2]V_2O_6\cdot 2H_2O$ (3) (BBTZ = 1,4-bis-(1,2,4-triazol-1-ylmethyl) benzene), were synthesized as electrocatalysts for OER. These MOFs can maintain structural stability when soaking in 1 mol/L KOH electrolyte, but the transformation of the structures of these MOFs only occurs on their electrode surfaces to form the V-doping metal oxyhydroxides as OER-active species during the electrocatalytic reaction. This proves that POVs were not active sites but precursors for the evolution of OER active species.

Overall, the electrocatalytic performance of the V/M-MOFs for HER and OER is superior to that of the monometallic V-MOFs, especially when combined with

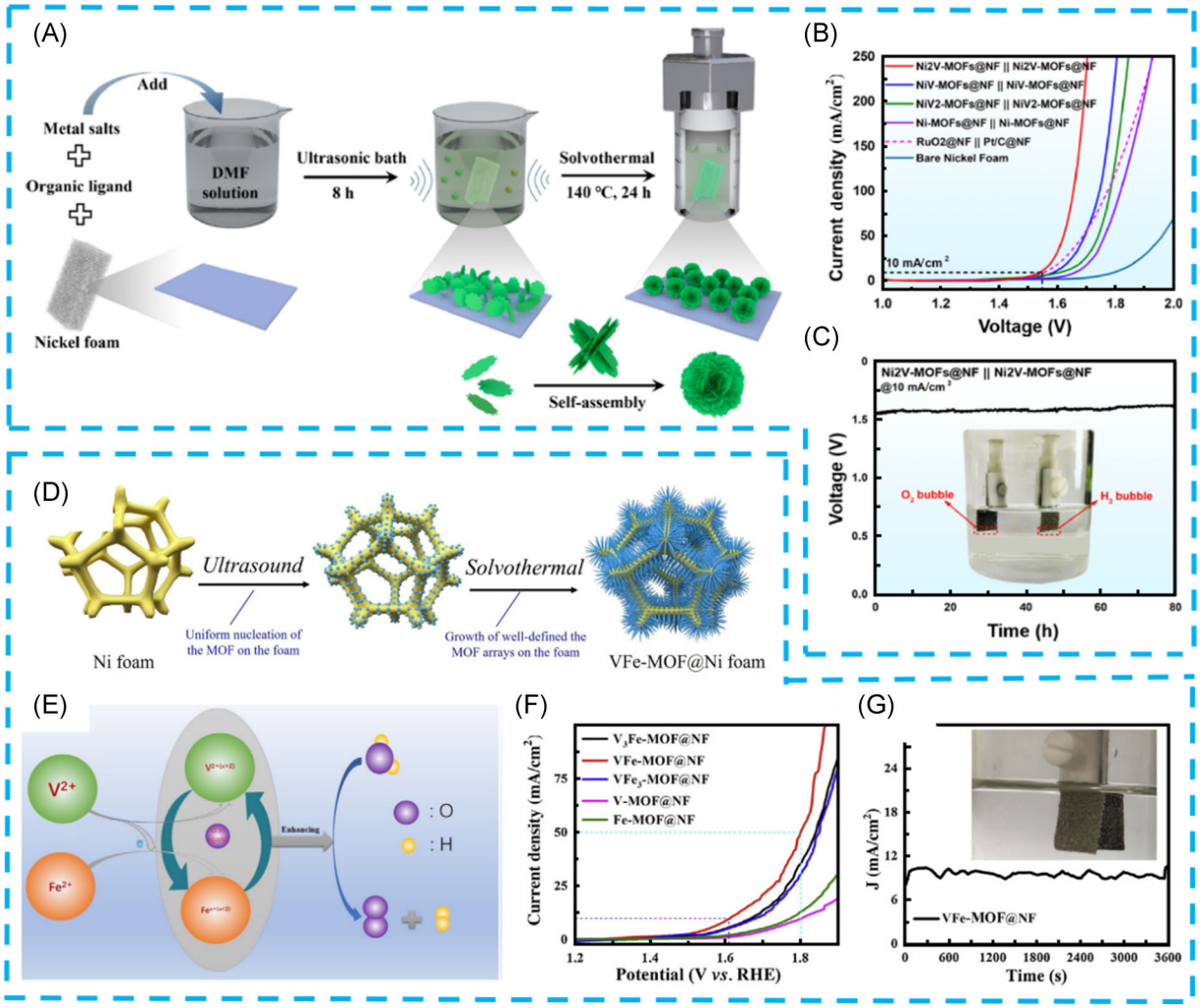

FIGURE 5 (A) A schematic diagram for growing Ni_2V-MOFs on a nickel foam substrate by ultrasound and solvothermal methods. (B) LSV curves for synthetic samples for overall water splitting. (C) Chronopotential curve of Ni_2V-MOFs@NF at a current density of 10 mA/cm^2 for 80 h and the inset is a photograph of the electronic cell. Reproduced with permission: Copyright 2020, American Chemical Society.[112] (D) A schematic for the formation of V/Fe-MOF@NF. (E) A schematic illustration of the synergistic effect between V and Fe in V/Fe-MOF@NF. (F) LSV curves of V/Fe-MOF@NF as anode and cathode catalyst in 1 mol/L KOH for overall water splitting. (G) The current-time (*I-t*) curves of V/Fe-MOF@NF at the constant potential for 3600 s (inset: An optical photograph for overall water splitting reaction in a two-electrode configuration). Reproduced with permission: Copyright 2021, Elsevier B.V.[113] MOF, metal-organic frameworks; Ni_2V-MOFs@NF, nickel-vanadium-based MOFs supported on nickel foam

the active metal (M = Ni, Fe). The comparison between Ni_2V-M-MOFs and POV-MOFs reveals that V/M-M-MOFs with nanosheet morphology have better electrocatalytic performance. Therefore, in addition to the synergistic effect between metals, morphology control also has an important influence on electrocatalytic performance.

4.2 | V-MOFs derivatives as electrocatalysts

Partial or full conversion of MOFs to metal carbon composites is a promising solution to enhance the conductivity and stability of electrocatalyst rather than using MOFs directly as electrocatalysts.[60,61,170] By controlling the heat treatment process of the original MOFs, the organic ligands can be graphitized to a certain extent, maintaining the original morphologies, and improving their conductivity dramatically. Moreover, the metal sites of the derivatives can achieve better catalytic activity and more exposed active regions when their ligands were removed.

As has been reported by Zhou et al.[171] and Yang et al.,[172] some V-doped electrocatalysts exhibit excellent electrocatalytic properties, in which V-doping can accelerate the electron transfer. For MOF-V-Ni_3S_2/NF, as a V-doped MOFs derivative, it requires low overpotentials

of 268 mV@10 mA/cm^2 and 118.1 mV@10 mA/cm^2 for OER and HER, respectively.[163] Due to the inherently large surface areas, exposed active site rate and improved charge collection of MOF-V-Ni_3S_2/NF, its catalytic performance is superior to that of the directly prepared V-Ni_3S_2/NF. ZIF-67 (ZIF stands for zeolitic imidazolate frameworks) is one of the more popular MOFs precursors to synthesize heteroatom-doped porous nanocarbon skeletons.[173,174] CoVO/C[164] and V-Co_xP@NC[165] are V-doped ZIF-67 derivatives that were successfully synthesized by different materials design strategies. For the former, it was synthesized by just a two-step process. The process started with the use of molecular vanadium oxide clusters embedded in ZIF-67 to prepare crystalline Co-V-oxide nanoparticles embedded in a layered nitrogen doped porous carbon matrix (Figure 6A). This then delivered higher activity for OER with an overpotential of 350 mV (at 10 mA/cm^2) and a Tafel slope of 75 mV/dec compared with the pyrolyzed pure ZIF-67 reference (Figure 6B,C).[164]

Whereas for the V-Co_xP@NC,[165] it can be obtained by low temperature phosphating of V-ZIF-67 synthesized by the partial ligand exchange of the as-prepared ZIF-67 and $NaVO_3$ (Figure 7A). The interaction between V and Co_xP can adjust the electronic structure of Co active sites and produce lattice distortions, which then promotes the catalysis of water splitting. The results showed that V-Co_xP@NC requires a small cell voltage of 1.54 V at current density of 10 mA/cm^2 to maintain the current density at 10 mA/cm^2 with slight fluctuation after the 20 h test (Figure 7B,C). Gopi et al.[166] reported that V-doped nickel-iron bimetallic nanoarrays (V-Ni_xFe_y-MOF@GO) supported by carbon materials exhibited excellent electrocatalytic performance for OER and HER in both acidic and alkaline media. For V-Ni_xFe_y-MOF@GO, the unique nanoparticles had been fabricated by carbonization of the as-prepared MOFs materials. The carbon in the structure can promote rapid ion diffusion, high conductivity and high catalytic activity, and V-doping can not only play a strong synergistic role with Ni/Fe, but also significantly increase the corrosion potential of electrocatalyst surface.

Apart from water splitting, the studies of V-MOFs derivatives on ORR have also been widely studied. Zhang et al.[175] reported the preparation of the porous Co-V-N/NC nanocomposite, which constitutes cobalt-vanadium nitride (Co-V-N) confined in nitrogen-doped porous carbon (NC) (Figure 8A). In addition to various accessible active sites at the phase boundaries, Co_4N, VN, and NC derived from ZIF-67 are also conducive to achieve effective charge transfer and mass transport. In addition, the electrical conductivity of electrocatalysts can be improved due to the incorporation of metallic Co_4N and VN (Figure 8B). The as-prepared Co-V-N/NC electrocatalysts exhibited excellent ORR performance with a limiting current density of 6.1 mA/cm^2, and the onset and half-wave potentials of 0.98 and 0.85 V, respectively due to the strong synergistic coupling effect among multi-components (Figure 8C). Moreover, Co-V-N/NC nanocomposites were more durable and methanol-resistant

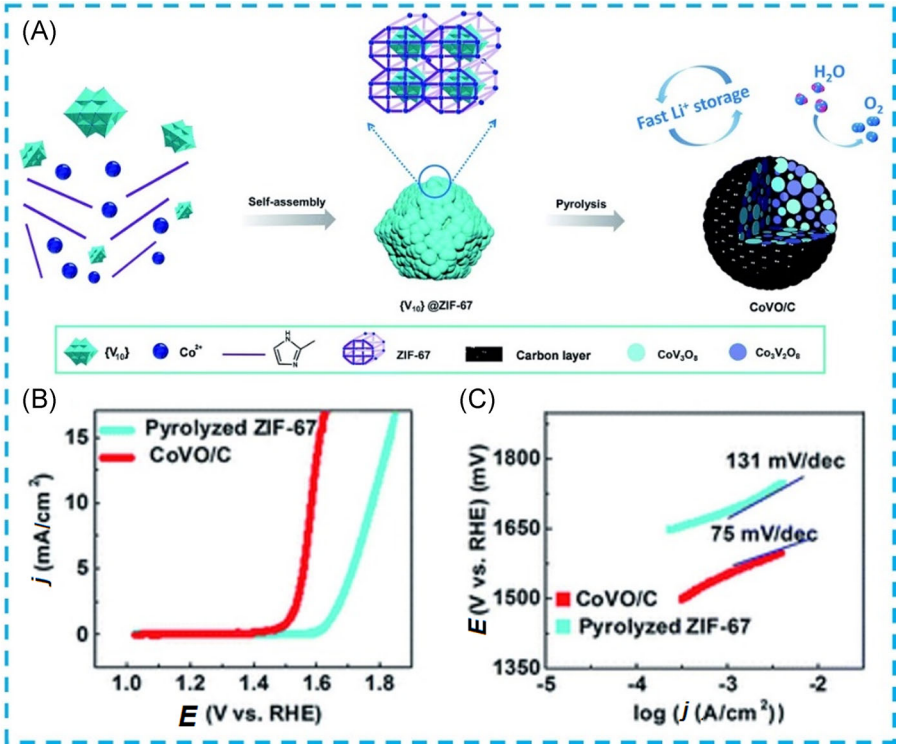

FIGURE 6 (A) An illustration of the two-step fabrication process of CoVO/C composite. (B) LSV polarization curves and (C) Tafel plots of CoVO/C, and the pyrolyzed ZIF-67 reference in 1.0 mol/L aqueous KOH for the OER. Reproduced with permission: Copyright 2019, Royal Society of Chemistry.[164] OER, oxygen evolution reaction

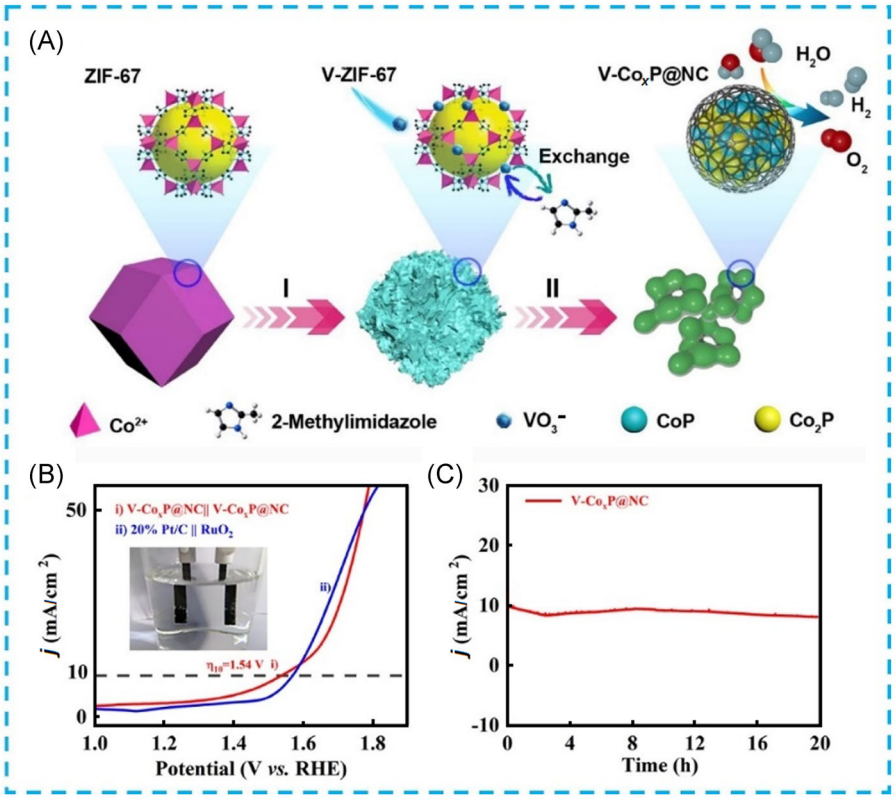

FIGURE 7 (A) A schematic illustration of V-Co$_x$P@NC NPs fabrication. (B) LSV curves of the V-Co$_x$P@NC | | V-Co$_x$P@NC and 20% Pt/C | | RuO$_2$ electrolytic system in alkaline solution. (C) The *i–t* curve of V-Co$_x$P@NC NPs. Reproduced with permission: Copyright 2020, Elsevier B.V.[165]

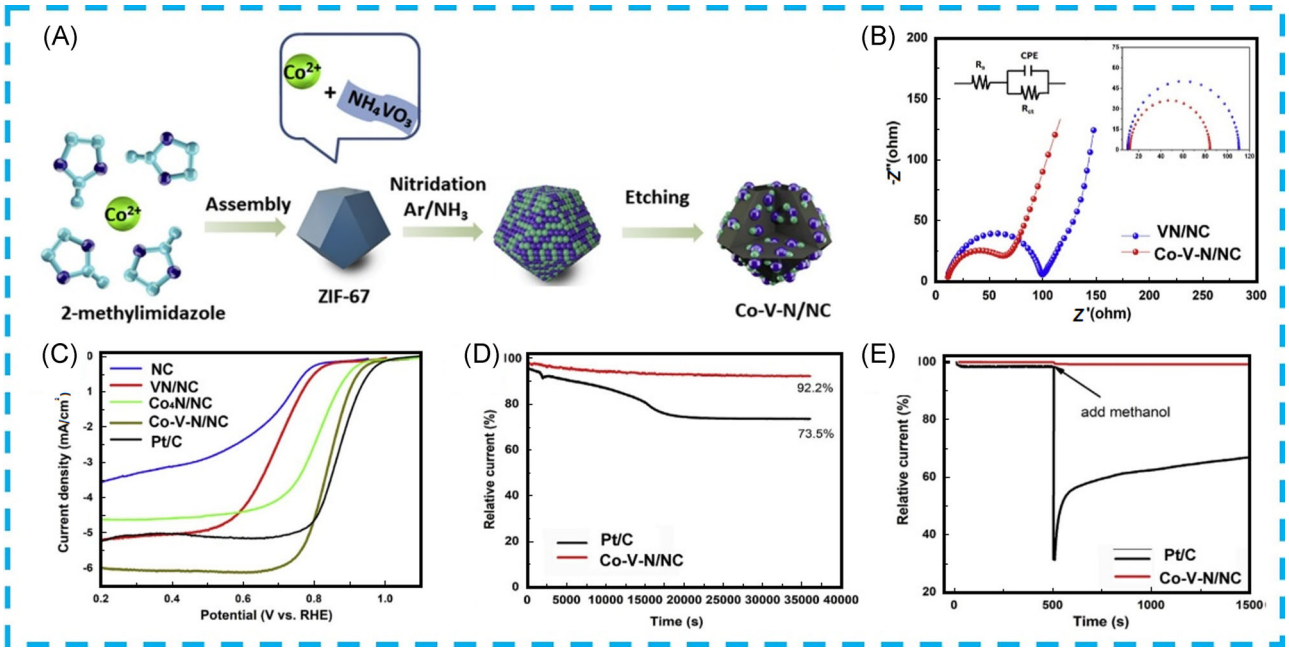

FIGURE 8 (A) A schematic illustration of the synthetic process of Co-V-N/NC. (B) Nyquist plots of the Co-V-N/NC and VN/NC recorded in O$_2$-saturated 0.1 mol/L KOH, inset is the equivalent circuit. (C) LSV curves of Co-V-N/NC and commercial Pt/C in an O$_2$-saturated 0.1 mol/L KOH with a scan rate of 10 mV/s and rotating speed of 1600 r/min. (D) Current-time (*i-t*) chronoamperometric responses of Co-V-N/NC and Pt/C obtained at −0.35 V (vs. Ag/AgCl) in O$_2$-saturated 0.1 mol/L KOH. (E) *i–t* curves of Co-V-N/NC and Pt/C at −0.35 V before and after adding 3 mol/L methanol. Reproduced with permission: Copyright 2019, Elsevier B.V.[175]

compared to the commercial Pt/C catalyst (Figure 8D,E). Muthurasu et al.[176] reported the synthesis of iron-doped metal-organic framework assisted cobalt vanadate integrated with cobalt oxide (Fe doped MOF CoV@CoO nanoflakes) via a facile synthetic approach. This approach synthesized a unique nanoflakes heterostructure, an abundant porous structure, high specific surface area, as well as extremely large active sites. Interestingly, the resulting Fe doped MOF CoV@CoO nanoflakes can be used trifunctional electrocatalyst for energy conversion such as ORR, OER, and HER, which produced very low overpotential and Tafel slope values. Electrocatalytic test results show that two-electrode water-splitting devices can exhibit 1.53 V at the current density of 20 mA/cm^2. Besides, portable rechargeable zinc-air battery was further assembled by employing specifically designed multifunctional electrocatalysts that can attain open-circuit voltage of 1.456 V, a power density of 138 mW/cm^3, and excellent cyclic stability, which is superior to Pt/C systems.

Compared with V-MOFs electrocatalysts, V-MOFs derivatives have the advantage of improving the electrocatalytic stability and conductivity, mainly due to the generation of some inorganic nanoparticles such as metal oxides or alloys during pyrolysis, as well as some highly conductive carbon materials. However, it is worth noting that the heat treatment of V-MOFs often leads to the aggregation of metal atoms, reducing the number of active sites in the catalyst to some extent. Therefore, the precise control of pyrolysis conditions is particularly important for the application of V-MOFs derivatives.

5 | ELECTROCHEMICAL ENERGY STORAGE

In recent years, electrochemical energy storage devices have achieved great success for the small portable electronic devices due to its environmental friendliness.[164] It is considered as one of the more promising ways to deliver clean energy sources to mitigate environmental issues and energy crisis.[177] To meet the market demand, energy storage devices are expected to exhibit higher power/energy density, longer service life, higher safety with lower manufacturing cost than before. Ever since the emergence of lithium-ion batteries, more efforts have been devoted to mitigating its inherent safety issues. The research of MOFs as electrode materials has garnered attention and developed rapidly in two aspects, one is that MOFs can be used directly as electrode materials by integrating electrochemical redox centers, and the other is MOFs derivatives with unique structures can be used in supercapacitors, and Li-based batteries (Li-ion, Li-S, and Li-O_2 batteries).[59] In this section, various V-MOFs and their derivatives for electrochemical energy storage will be segregated into these two aspects (Table 2).

5.1 | V-MOFs as electrode materials

5.1.1 | MOF-47 based materials

As an emerging energy storage device, supercapacitors have the advantages of large power density, fast charge and discharge rates and long cycle life.[186–188] Yan et al.[189] reported for the first time that MIL-47 was synthesized by a facile one-step solvothermal strategy and was used as an electrode material for supercapacitors. With that, it could exhibit relatively high capacity, long cycle life and high energy density. The MIL-47 synthesized by that mean yielded uniform rods with a length of 0.5−3 μm and a width of 200 nm, and it exhibited a large specific surface area of 116 m^2/g with an average pore diameter of 3.6 nm. With that, it then promotes better diffusion of ions and electrolytes, thus improving the electrochemical performance (Figure 9A,B). The MIL-47 electrode exhibited a maximum specific capacitance of 572.1 F/g at current density of 0.5 A/g and 520.8 F/g at 1 A/g, yet still able to retain 92.8% of the capacity after 1000 cycles (Figure 9C,D). The probable reactions can be described as the equation of V^{IV} (O) (bdc) + xNa$^+$ + xe$^-$ ↔ Na$_x$$V^{IV}$ (O) (bdc). Furthermore, both aqueous and solid-state asymmetric supercapacitors can be successfully assembled by rod-like MIL-47 and activated carbon. After 10,000 charge–discharge cycles, the specific capacitance of aqueous and solid-state devices can be maintained at 92.1% and 93.6%, respectively, which revealed outstanding cycling stability (Figure 9E,F). For the solid-state device, it exhibited a remarkable energy density of 6.72 mW·h/cm^3 at a power density of 70.35 mW/cm^3. The superior performance proved that V-MOFs electrodes have the potential to be used as active materials in supercapacitors.

In 2019, He et al.[178] have reported the direct growth of 3D conductive MIL-47 nanowire-bundle arrays on carbon nanotube fibers (CNTFs) via a time-dependent solvothermal reaction. The products were synthesized with varying reaction times of 12, 24, 48, and 60 h, and were denoted as V-MOF-12, V-MOF-24, V-MOF-48, and V-MOF-60, respectively (Figure 10A). It was then used as the cathode for Zn-ion (V-MOFs//Zn) batteries. Based on their experimental results, the optimized V-MOF-48 obtained the highest volumetric capacity of 101.8 mA·h/cm^3 at a current density of 0.1 A/cm^2 and achieved the best rate capability in an aqueous electrolyte amongst the variants (Figure 10B,C). In this study system, the performance of all-solid-state fiber-shaped V-MOF//Zn battery assembled by poly(vinyl alcohol) (PVA) electrolyte

TABLE 2 Comparison of the performance of V-MOFs and their derivatives for energy storage

MOFs/Precursors	Electrode materials	Batteries	Current density	Cycle number	Specific capacity	Refs.
V-MOFs:						
MIL-47	MIL-47 nanowire bundle arrays	Zn-ion	100 mA/cm^2	400	101.8 mA·h/cm^3	178
MIL-47	MIL-47 nanorods	Zn-ion	100 mA/g	70	320 mA·h/g	179
MIL-100	S@MIL-100	Li-S	0.1 C	200	550 mA·h/g	180
	S@MIL-100/rGO	Li-S	0.1 C	75	650 mA·h/g	
V/Fe PBAs	$Na_{0.4}(VO)_3[Fe(CN)_6]_2{\cdot}12H_2O$	Na-ion	110 mA/g	250	55 mA·h/g	181
V-MOFs derivatives:						
MIL-88B	V_2O_3/C	Na-ion	2000 mA/g	1000	181 mA·h/g	146
MIL-88B	V_2O_5	Li-ion	50 mA/g	100	324 mA·h/g	147
MIL-88B	a-V_2O_5@C	Zn-ion	40 A/g	20,000	249.2 mA·h/g	149
V-NDC	VO_x/PCs	Na-ion	500 mA/g	2000	153 mA·h/g	150
MIL-101	$Li_3V_2(PO_4)_3$	Li-ion	1 C	1000	105.8 mA·h/g	151
Co-V-MOF	Sponge-like $Co_3V_2O_8$	Li-ion	1 000 mA/g	700	501 mA·h/g	152
Co-V-MOF	Porous $Co_3V_2O_8$	Li-ion	1 000 mA/g	100	940 mA·h/g	154
V-NDC	V_2O_3/N-doped porous carbon nanorods	Na-ion	1 000 mA/g	3000	134.5 mA·h/g	182
MIL-47	V_2O_3/C/S	Li-S	1 C	1000	598 mA·h/g	183
V-MOF-GFDW	$Li_3V_2(PO_4)_3$/P-C	Li-ion	10 C	1100	65 mA·h/g	184
V-MOF-SLS	$Na_3V_2(PO_4)_3$ sheets	Na-ion	200 C	6000	40 mA·h/g	185

Abbreviations: GFDW, glass fiber drawing wastewater; MOF, metal-organic framework; NDC, 1,4-naphthalene dicarboxylates; SLS, sodium ligninsulfonate.

has also been investigated (Figure 10D), it can deliver a high energy density of 17.4 mW·h/cm^3 while maintaining a high power density of 1.46 W/cm^3. The galvanostatic charge-discharge curves at various current densities show that the specific capacity in the PVA electrolyte is similar to that in the aqueous electrolyte at a low current density (0.1 A/cm^2), and it still retained 56.9% of initial capacity when the current density was increased 50-fold (Figure 10E,F). In addition to the applications mentioned above, Ru et al.[179] recently have focused on the use of MIL-47 in conventional aqueous button batteries. The layered MIL-47 nanorods synthesized via one-step hydrothermal method are utilized as the cathode material for the aqueous MOF-Zn battery, which show high initial specific capacity of 320 mA·h/g at 0.1 A/g, as well as the desirable rate capability and cycling performance.

5.1.2 | MOF-100 based materials

As one of the core battery technologies in the post-lithium-ion era, Li-S batteries (LSBs) have attracted a lot of research interests due to their high theoretical capacity (≈1675 mA·h/g for S and ≈3860 mA·h/g for metallic Li) and energy density (≈2500 W·h/kg considering complete reaction to Li_2S) in recent years.[190,191] However, the shuttle effect of polysulfides in their batteries and the reduction of Li_2S or Li_2S_2 products hampered their practical application, thus great efforts have been made to develop advanced cathode materials to alleviate these problems.[192,193] When employed in Li-S batteries, MOFs can be either as host materials to host the sulfur and confine the polysulfides, or as separators to prevent the migration of polysulfides to anode side, which can facilitate electron transport and capture of soluble polysulfide.[194–196] Hou et al.[180] reported for the first time that mesoporous MIL-100(V) and MIL-100(V)/reduced graphene oxide (rGO) composites can be used as sulfur cathode hosts for Li-S batteries. In the crystal structure of MIL-100(V), there is also a small percentage of V^{4+} in addition to a large amount of V^{3+} in vanadyl groups, which provide different Lewis acid sites and form strong interactions with sulfur and lithium polysulfides (Figure 11A). MIL-100(V) and MIL-100(V)/rGO are grounded with sulfur in a certain proportion, respectively. The mixture is then heated to obtain S@MIL-100(V) and S@MIL-100(V)/rGO, both of

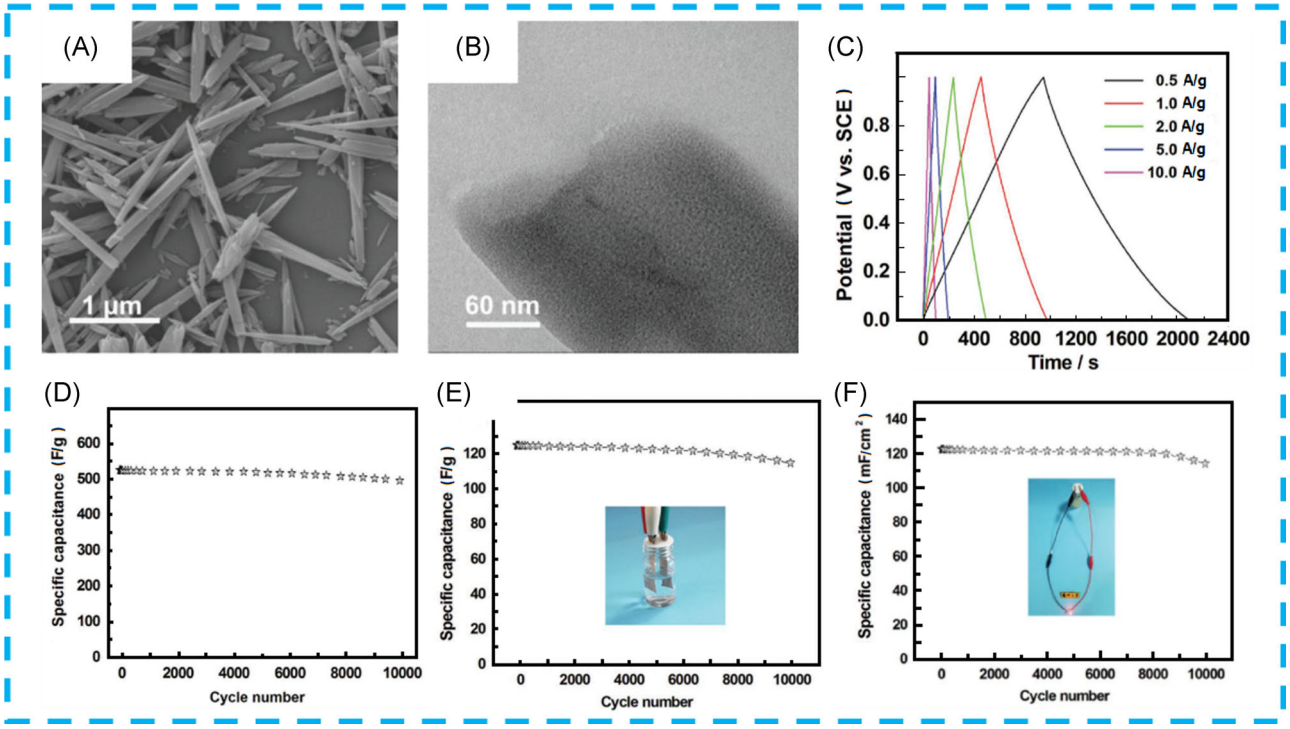

FIGURE 9 (A) Field emission scanning electron microscopy (FE-SEM) and (B) high resolution transmission electron microscope (HRTEM) images of as-prepared MIL-47. (C) The galvanostatic charge-discharge curves of rod-like MIL-47 electrode at different current densities. (D) Charge–discharge cycling curve at a current density of 1 A/g in 1.0 mol/L Na_2SO_4 electrolyte. (E) Charge–discharge cycling curve of the rod-like V-MOF//activated carbon aqueous device at a current density of 1 A/g. (F) Charge-discharge cycling curve of the rod-like V-MOF//activated carbon solid-state device at a current density of 2 mA/cm^2. Reproduced with permission: Copyright 2018, Wiley-VCH.[189] V-MOF, vanadium metal-organic frameworks

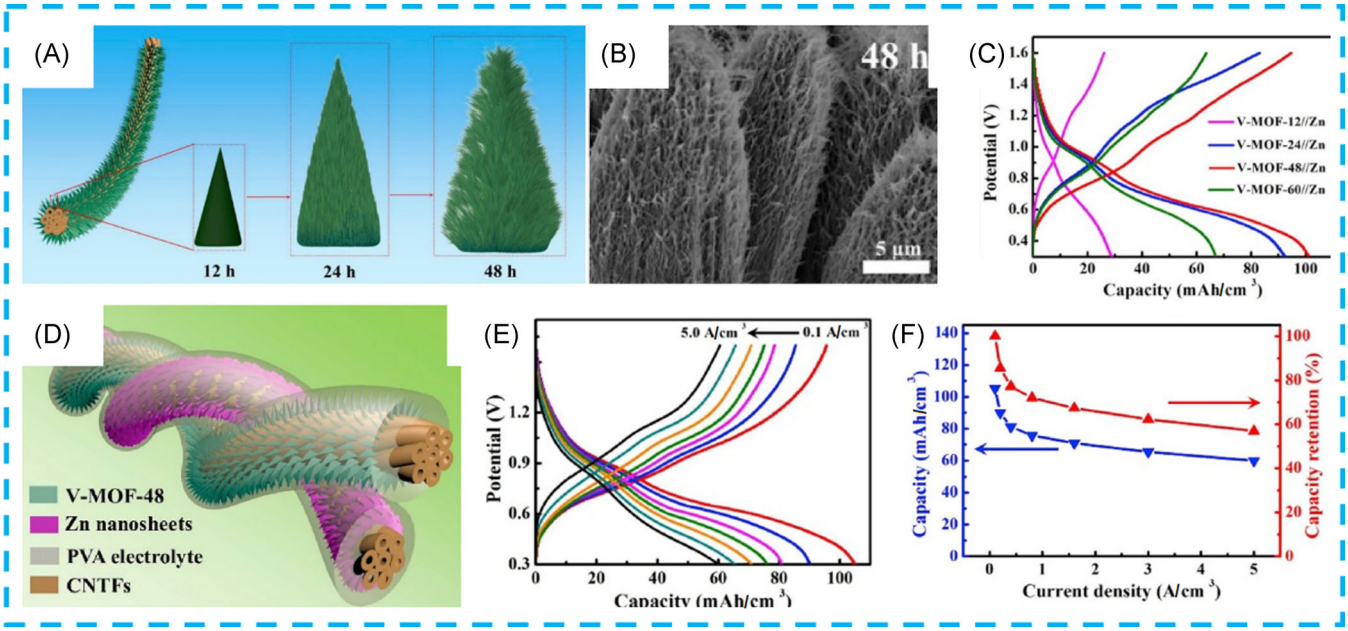

FIGURE 10 (A) An illustration of the preparation process for the V-MOF@CNTF with hierarchical nanowire structure. (B) SEM image of V-MOF-48. (C) The galvanostatic charge-discharge curves at a current density of 0.1 A/cm^2 for V-MOF-12//Zn, V-MOF-24//Zn, V-MOF-48//Zn, and V-MOF-60//Zn. (D) An illustration of the all-solid-state fiber-shaped V-MOF-48//Zn battery. (E) Galvanostatic charge-discharge curves and (F) specific capacities of the fiber-shaped V-MOF-48//Zn battery at various current densities. Reproduced with permission: Copyright 2019, Elsevier B.V.[178]

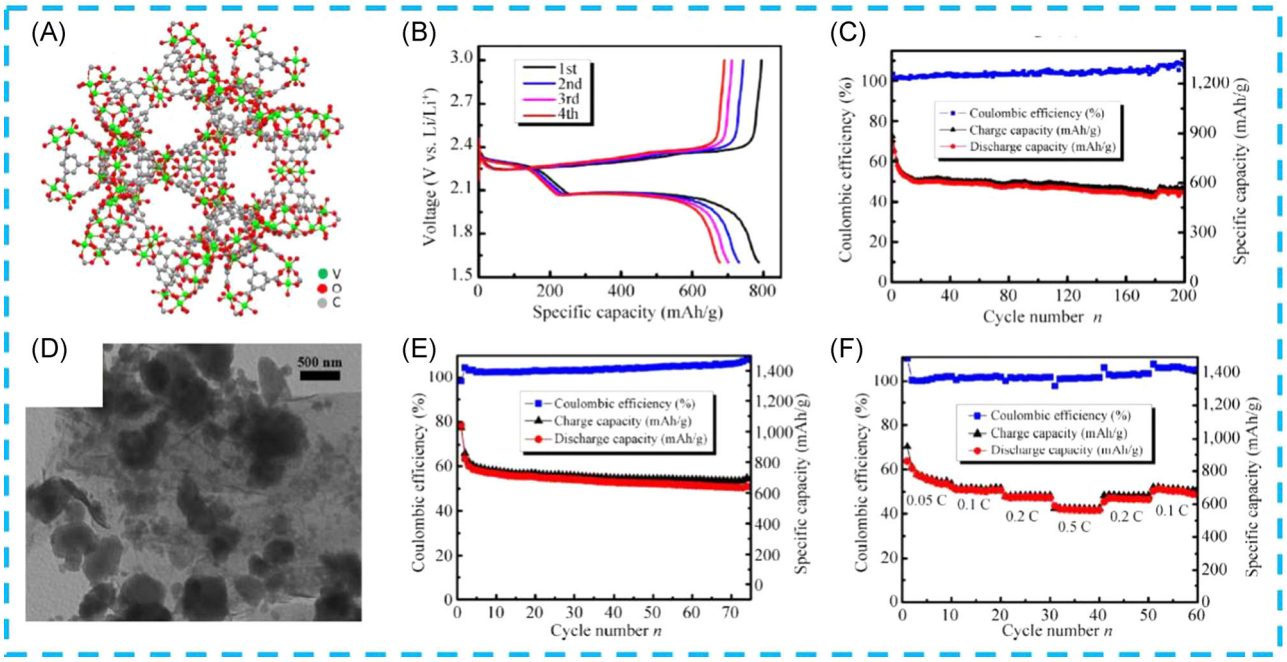

FIGURE 11 (A) Crystal structure of MIL-100(V) (vanadium, carbon, and oxygen atoms are depicted as green, gray, and red spheres, respectively). (B) Galvanostatic discharge/charge profiles of S@MIL-100(V). (C) Cycling performance of S@MIL-100(V) at a current of 0.1 C. (D) TEM image of S@MIL-100(V)/rGO. (E) Cycling performance of S@MIL-100(V)/rGO at a current of 0.1 C. (F) Rate performance of S@MIL-100(V)/rGO at 0.05, 0.1, 0.2, and 0.5 C. Reproduced with permission: Copyright 2017, Springer Nature Limited.[180] TEM, transmission electron microscope

which show excellent electrochemical performance for Li–S batteries. When tested at 0.1 C, the initial charge and discharge capacities of S@MIL-100(V) were 879 mA·h/g and 849 mA·h/g, respectively. In addition, the capacity was maintained at 550 mA·h/g after 200 cycles (Figure 10B, C). This proves that the diffusion of lithium polysulfides has been effectively controlled. For S@MIL-100(V)/rGO, most of the sulfur-containing MIL-100(V) particles are attached to reduced graphene oxide flakes (Figure 11D), and the reversible capacity was maintained at 650 mA·h/g after 75 cycles at a current density of 0.1 C (Figure 11E). While, the specific capacity of S@MIL-100(V)/rGO attenuated slowly when the current density was increased from 0.05 to 0.5 C, and the specific capacity at 0.5 C was still 570 mA·h/g (Figure 11F). With the aforementioned results, it shows that the sulfur loading and cycling stability can be improved when V-MOFs are applied as sulfur cathode hosts for Li–S batteries.

5.1.3 | PBAs-based materials

The discovery of Prussian blue can be traced back to 1704.[197] Early work by Neff et al. in the 1980s demonstrated the exceptional electrochemical activity and ionic permeability of Prussian blue crystals, which has led to the widespread use of PBAs in batteries to date.[198,199] Although the excellent crystal structure and simple diffusion kinetics of PBAs, the capacity delivered in aqueous systems has been limited to less than about 60 mA·h/g. The electrochemical process of PBAs is mainly controlled by the electrochemical process of metal ions inserting/extracting the ions. So, the optimization of the transition metal ions combination is particularly important. Lee et al.[181] prepared a novel PBAs ($Na_{0.4}(VO)_3[Fe(CN)_6]_2{\cdot}12H_2O$, V/Fe PBAs) by a facile co-precipitation method for aqueous rechargeable batteries, where V and Fe ions are conductive to the multiple-electron energy storage process (Figure 12A). With that, the V/Fe PBAs have exhibited capacity of 91 mA/h under a current density of 110 mA/g, even the capacity of the 250th cycle was still at 55 mA/h (Figure 12B). In addition, with its open structure and 3D hydrogen bond network, the V/Fe PBAs exhibited a relatively high capacity of 54 mA·h/g under an extremely high current density of 3520 mA/g (Figure 12C). Additionally, the specific capacity also exhibited highly stable performances. Long-term cyclic stability results show that the capacity retention was 80% and 79% after 250 cycles for current densities of 880 and 1760 mA/g, respectively (Figure 12D). However, the capacity decreased more rapidly in the initial cycle due to the dissolution of vanadium ions. Inhibition of the dissolution and enhancement of

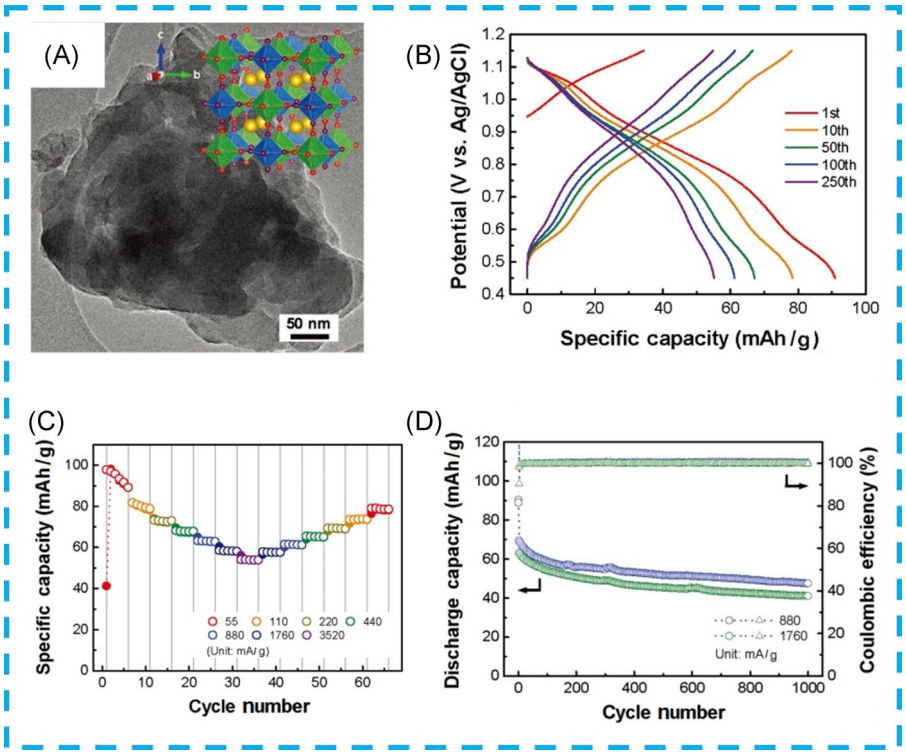

FIGURE 12 (A) Low-magnification TEM image of the cathodes synthesized by co-precipitation (with HCl). Inset is the crystallographic structure of V/Fe PBA (yellow, blue, green, red, and purple spheres represent Na, V, Fe, C, and N, respectively). (B) Potential profiles of the cathodes synthesized by co-precipitation (with HCl), evolving over 250 cycles (potential range: 0.45–1.15 V versus Ag/AgCl, charge/discharge current density: 110 mA/g). (C) Specific capacity of the charge (filled circle) and discharge (open circles) process for the V/Fe PBA cathodes measured under various charge/discharge current densities ranging from 55 to 3520 mA/g. (D) Discharge capacity and Coulombic efficiency as a function of the cycle number with a charge/discharge current density of 880 and 1760 mA/g, respectively. Reproduced with permission: Copyright 2017, Wiley-VCH.[181] PBA, Prussian blue analogues; TEM, transmission electron microscope

reaction kinetics of V ions are effective measures to circumvent the dramatic electrochemical performance deterioration. Additionally, those measures can also improve the electrochemical performance of V/Fe PBA, such as the introduction of mixed conductor coating. With the similar open framework structures and huge interstitial sites to PBAs, a series of metal-organic phosphate open framework (MOPOF), $A_2[(VO)_2(HPO_4)_2(C_2O_4)]$ (A = Li, Na, or K) as cathodes for hybrid LIBs[200,201] and KIBs[202] have also been widely reported by Vittal's and Chen's group. The diffusion channels for Li or other alkali ions can deliver highly reversible storage capacities, and it may give a new direction to design and develop cathode materials.

As mentioned above, V-MOFs as electrode materials can improve electrochemical energy storage performance in three aspects: (1) The high specific surface area of V-MOFs can improve ion transport property during energy storage processes; (2) Its open-framework crystal structure can also accommodate appropriate space for ion storage and electrochemical reactions; and (3) Vanadium ions with different valance states can provide various Lewis acid sites and form stronger chemical interactions with guest ions.

5.2 | V-MOFs derivatives as electrode materials

In general, the direct usage of V-MOFs as electrode materials was rarely studied due to the poor electrical conductivity and their complicated energy storage mechanisms of MOFs. For MOFs, there are mainly two types of energy storage: pore reversible energy storage and reversible chemical reaction energy storage. For LIBs, the reversible de-intercalation of lithium ion in pores of MOFs belongs to the mechanism of pore reversible lithium storage, while the organic ligands in the MOFs structure provide insertion sites for lithium ions.[203] It is noteworthy that the structure of MOFs would dissolve or collapses after the process of charging and discharging, the resulting solid then (which may be vanadium oxide or carbon) continues the subsequent

lithium storage process. The lithium storage mechanism is then transformed into reversible chemical reaction, which refers to the occurrence of reversible chemical reaction at the electrode, and lithium ion replaces vanadium ion to form new vanadium-based compounds. This energy storage mechanism has inspired researchers to continuously develop and exploit the precursor V-MOFs, especially the MOFs derivatives in energy storage has received widespread attention.

5.2.1 | Vanadium oxide/vanadium oxide@C

When V-MOFs are used as precursors, the self-templating method is proved to be a convenient and effective way to achieve the conversion of V-MOFs to vanadium oxides. Among the plentiful vanadium oxides, vanadium sesquioxide (V_2O_3) shows typical corundum-type structures with a spatially symmetric of $R\bar{3}c$, the oxygen atoms occupy the six vertices of the vanadium atom centered octahedron, and every two VO_6 octahedrons share an edge, thus producing a special pore and a suitable pore diameter distribution. The resulting features then help in accelerating the de-intercalation of ions and improve the rate capability. In addition, the porous carbon derived from organic ligands coated on the surface can further improve the cycle life of the electrode material. Therefore, the carbon-coated V_2O_3 (V_2O_3@C) derived from V-MOFs has attracted much attention of many researchers due to the advantages in composition and structure.[146–150]

When MIL-88B(V) was used as precursor, the porous shuttle-like vanadium oxides (V_2O_5, V_2O_3/C) were successfully prepared through a particular calcining process, in which V_2O_5 and V_2O_3/C were obtained by calcination in air and Ar atmosphere, respectively (Figure 13A).[146] In terms of morphology, both V_2O_5 and V_2O_3/C retained a prismatic structure like MIL-88B(V), whereas abundant

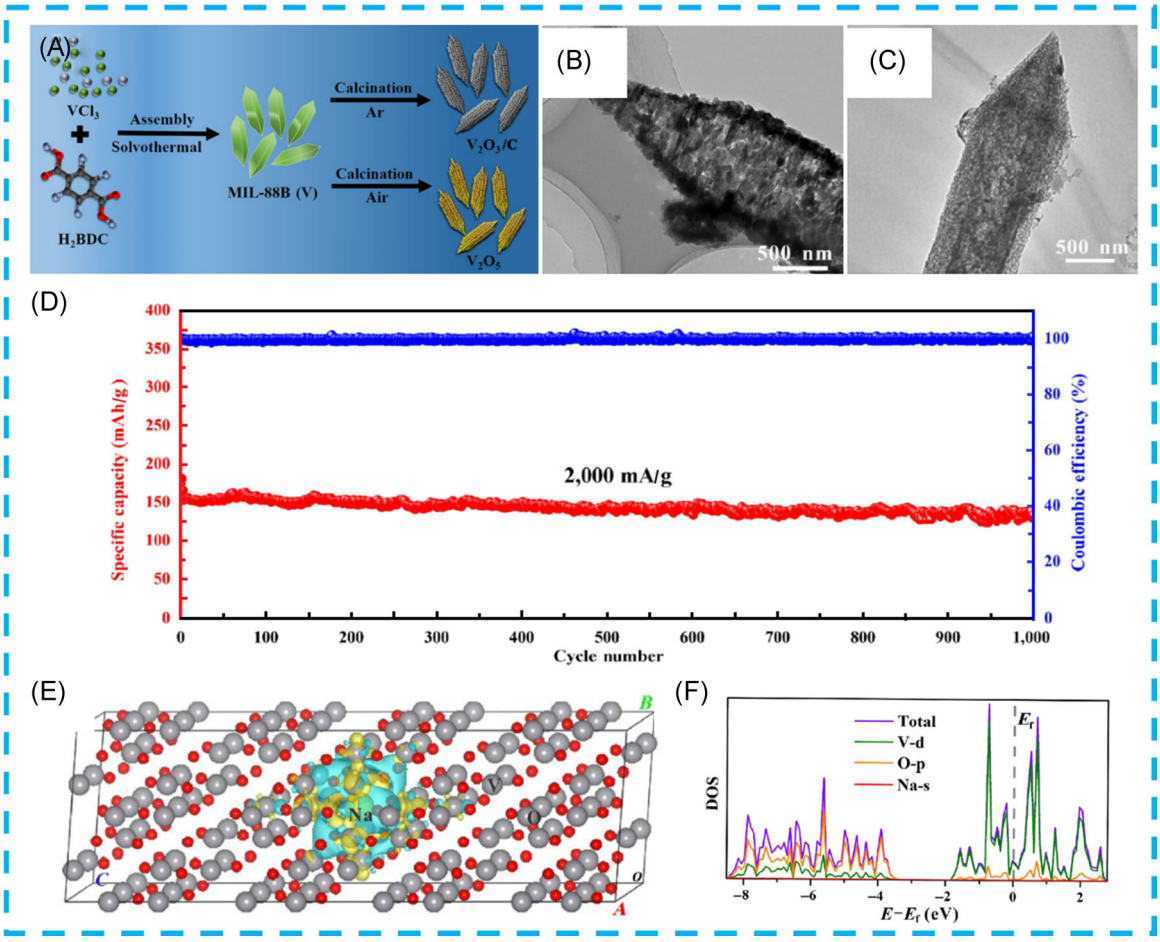

FIGURE 13 (A) An illustration of preparation process for the shuttle-like porous V_2O_3/C and V_2O_5. TEM images of the shuttle-like (B) V_2O_5 and (C) V_2O_3/C. (D) The high-rate (2000 mA/g) cycling performance and corresponding Coulombic efficiency of V_2O_3/C. (E) Charge-density differences of V_2O_3 with one Na atom inserted. (F) Calculated density of states (DOS) for V_2O_3 after Na ion insertion. Reproduced with permission: Copyright 2018, Springer Nature Limited.[146] TEM, transmission electron microscope

micropores were formed during calcination. V_2O_5 and V_2O_3/C exhibited hollow structure and porous structure, respectively (Figure 13B,C). The in-situ carbon layers can not only enhance the electronic conductivity of vanadium oxides, but also allow full electrolyte penetration and rapid metal ion transport. In Figure 13D, V_2O_3/C exhibited excellent electrochemical properties when used as an anode material for SIBs. The specific discharge capacity can reach 181 mA·h/g at 2000 mA/g, and the capacity can still be retained at 133 mA·h/g, corresponding to a fading rate of 0.032% per cycle after 1000 cycles. Density functional theory (DFT) calculation results indicated that Na ions preferred to form Na−O chemical bond with O atoms, accompanied by obvious charge transfer. It can also be found that its good conductivity can be maintained after the insertion of Na ions (Figure 13E,F).[146]

Kong et al.[182] explored the effect of the introduction of ammonia treatment on vanadium matrix composites and their electrochemical properties in sodium ion capacitors (SICs). V_2O_3/N doped porous carbon (VNC-300) maintained the ultra-small size of V_2O_3 particles (~2.1 nm) in the process of low temperature nitridation, which was an excellent cathode material for sodium storage, and the optimized V_2O_3/N-doped porous carbon nanorods exhibited high specific capacity and excellent stability for sodium storage (Figure 14A). Most importantly, the SICs device based on active carbon as positive electrode and VNC-300 as negative electrode exhibited a good rate performance. The energy density values were from 63 to 38 W·h/kg at various current densities from 50 to 5.0 mA/g, and it exhibited an excellent energy density of 38.7 W·h/kg at a power density of 5805 W/kg (fast charge and discharge in 25 s) (Figure 14B). In 2018, this group also prepared vanadium oxide/porous carbon nanorods (VO_x/PCs) with oriented 2D pores by utilizing the thermally induced bond instability. The unstable bond between V and the coordination water was broken and a lot of

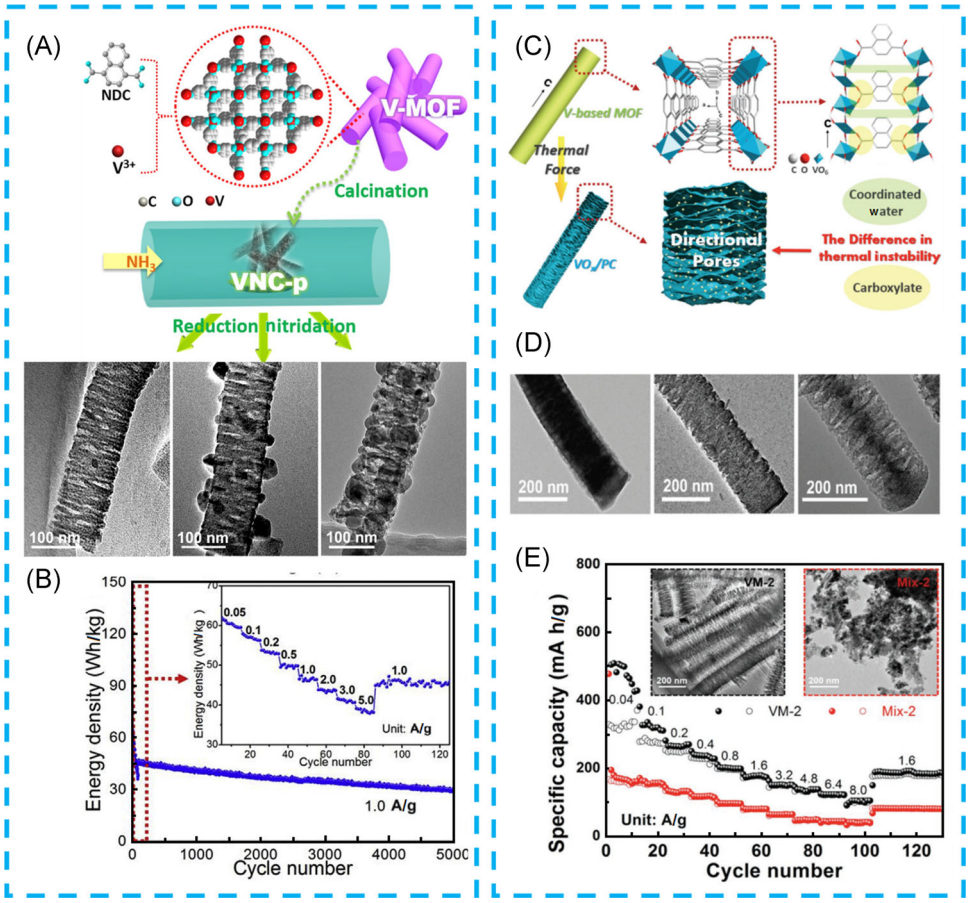

FIGURE 14 (A) An illustration of the structural change process of VNC-p via ammonia treatment. (B) Cycling performance of VNC-300//AC device at 1.0 A/g (inset: rate capability at various current densities). Reproduced with permission: Copyright 2018, Elsevier B.V.[182] (C) An illustration of the formation of hierarchical VO_x/PCs. (D) TEM images showing structural changes at VM-500 °C, VM-600 °C, and VM-700 °C. (E) Rate performance of VM-600 °C and the disordered contrast. Inset: TEM images of VM-600 °C and the disordered contrast, VM stands for vanadium-based MOF with the structure $[V(OH)(NDC)\cdot xG]_n$ (G = guest molecules, NDC = 1,4-naphthalene dicarbo-xylates). Reproduced with permission: Copyright 2018, Wiley-VCH.[150] TEM, transmission electron microscope

slit-like pores were formed perpendicular to the direction of crystal growth (Figure 14C,D).[150] When used as anode materials for sodium storage, it displayed a discharge capacity of 481.5 mA·h/g at the low current density of 0.04 A/g and delivered the prominent capacity of 93.8 mA·h/g at the high rate of 10.0 A/g (Figure 14E). The results show that composites with hierarchical porous architectures contribute to an increase in reactive surface area, thus improving rate capability and cycling life of sodium storage. Most importantly, it is relatively easy to construct laminated composites from MOFs, which provides new ideas for the design and preparation of high-performance electrode materials.

V-MOFs derived V_2O_3/C and V_2O_5/C have also been reported as intercalation cathode for aqueous zinc-ion batteries (ZIBs). These V-MOFs derivatives have unique channel, appropriate pore size distribution and abundant valence states that can shorten the ion transport distance which in turn improves the conductivity, equates to good electrochemical performance. Interestingly enough, MIL-88B(V) derived crystalline c-V_2O_3@C can be further converted into the composite of amorphous V_2O_5 and conductive carbon (a-V_2O_5@C) for aqueous ZIBs by electrochemical oxidation strategy (Figure 15A).[149] Although a-V_2O_5@C showed a similar morphology to c-V_2O_3@C, the V_2O_3 nanoparticles smash to amorphous V_2O_5 during the electrochemical induction process. With amorphous V_2O_5 and conductive carbon, a-V_2O_5@C possessed more active sites and offered more isotropic zinc ion diffusion routes, yielding fast speed of zinc ion transport and high discharge capacity (Figure 15B). The discharge capacity of a-V_2O_5@C reached 620.2 mA·h/g at 0.3 A/g, and Zn/a-V_2O_5@C batteries displayed a superior rate performance that maintained at 72.8 mA·h/g at a high current density of 200 A/g (2571 C) and excellent cycling performance of 20000 cycles (91.4% capacity retention) at 40.0 A/g (Figure 15C,D). Furthermore, the flexible soft-packaged Zn/a-V_2O_5@C batteries have also been studied

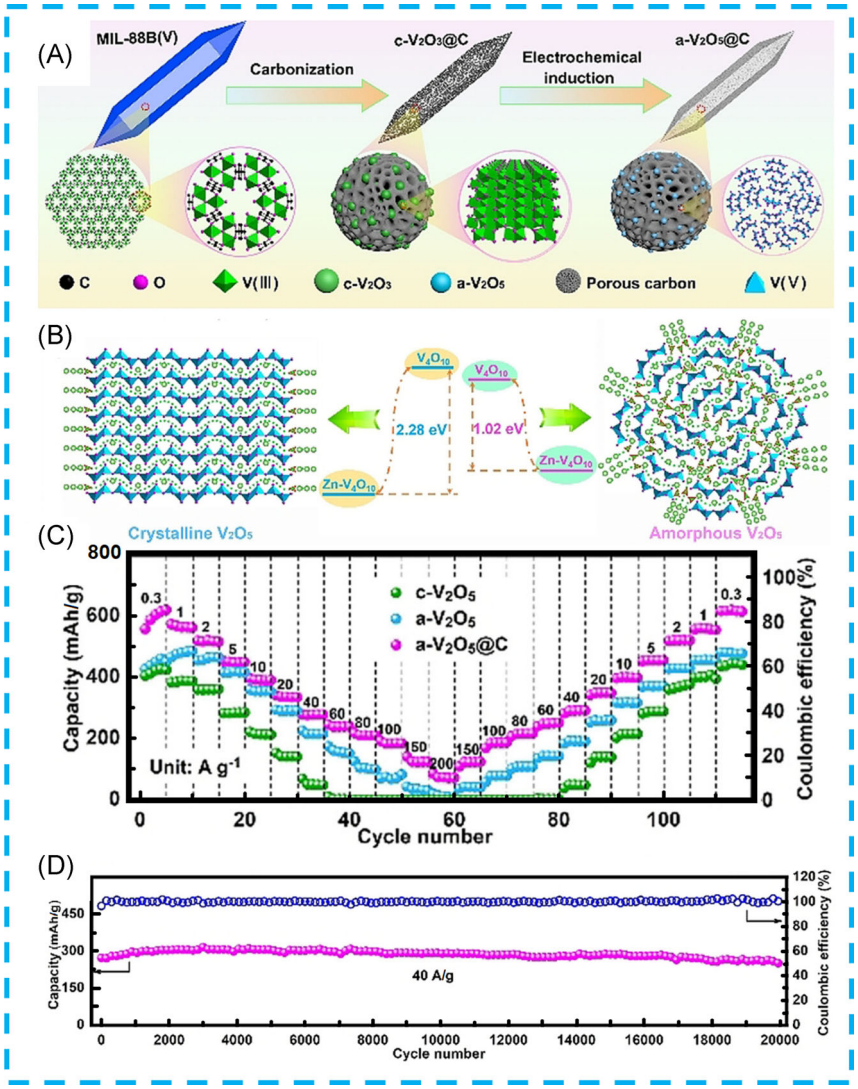

FIGURE 15 (A) Illustration of the fabrication process of vanadium oxide by calcination of MIL-88(V) precursor. (B) Illustration of Zn^{2+} diffusion and Zn^{2+} (de) intercalation energy in crystalline and amorphous V_2O_5 from first-principles calculations. Rate performance (C) and long-term cycle test (D) of a-V_2O_5@C. Reproduced with permission: Copyright 2020, Wiley-VCH[149]

and have shown to be a great prospect for the practical application of flexible energy storage devices.

Except for SIBs and ZIBs,[146,148–150,182,204] the V-MOFs derived V_2O_5 and V_2O_3@C for LIBs or LSBs have also been carefully studied. Different temperatures in air atmosphere (400 °C, 450 °C, 500 °C, 550 °C, 600 °C, 650 °C) have considerable influence on the morphology of the target product V_2O_5, and the size of the product tends to decrease with the increase of temperature.[147] Smaller materials with larger specific surface areas can be obtained at an appropriate temperature, thus increasing the contact area between the material and the electrolyte, which was conducive to the de-intercalation of lithium ions. The results of charge-discharge cycle showed that the performance of the samples calcined at 600 °C was better than that at other temperatures. However, the insufficiency was that the capacity gradually decreased within 100 cycles, it may be due to the gradual decrease of V_2O_5 during the cycle which hindered the de-intercalation of lithium ions and the adverse reactions of electrode materials and electrolytes. Yang et al.[183] developed a synthetic approach to prepare V_2O_3@C hollow micro-cuboid with hierarchical lasagna-like structure through calcining MIL-47 precursor, and then the V_2O_3@C/S composite was further synthesized by mechanically mixed V_2O_3@C and sulfur S. When used as a cathode material for LSBs, it showed superior cycling stability (62.3% after 1000 cycles at 1 C) and rate performance (665.6 mA·h/g at 2 C) at a relatively high sulfur loading of 3.7 mg/cm^2.

5.2.2 | Vanadate (mixed metal oxides [MMOs])

Transition metal oxides (TMOs) and MMOs as cathode materials for batteries have attracted much attention in recent years due to their high theoretical specific capacity, low price, good stability, as well as the synergistic influence of metal ions.[205–207] MMOs prepared by oxidative calcining of MOFs possess the superiorities of high energy density, high economic efficiency, and simple synthesis, greatly promoting the application in electrochemistry. In the past few years, some vanadium-centric, non-stoichiometric MMOs have shown potential applications in batteries, photocatalysis, and hydrogen storage.[208,209]

Soundharrajan et al.[152] successfully synthesized cobalt vanadate ($Co_3V_2O_8$) through pyrolysis of Co-V-MOFs network, which showed the well-defined sponge-like network morphology (Figure 16A). With the unique nanostructured morphology, the as-prepared $Co_3V_2O_8$ exhibited good cyclability of 700 cycles and specific capacity of 501 mA·h/g, respectively, at a current density 1000 mA/g (Figure 16B). While, in terms of stability, it can still retain an average capacity of 430 mA·h/g with Coulombic efficiency reaching close to 100% at the maximum current density of 3200 mA/g (Figure 16C). The research group also reported the preparation of $Co_3V_2O_8$ microspheres assembled with 20−50 nm particles from Co-V-MOFs precursor by one-pot method, which exhibited a higher discharge capacity and excellent reversible capacity for LIBs due to the synergistic effects between the metallic species.[154] Unlike Co-V-MOFs, nanoparticles were in situ generated and aggregated on the surface of the microspheres during the calcination process, and the large number of voids confirmed the porous structure of $Co_3V_2O_8$ (Figure 16D). When used as electrode material, it showed excellent cycling performance and rate performances under high current density (showing the specific discharge capacity of 940 mA·h/g after 100 cycles at 1 A/g with the Coulombic efficiency of nearly 100%) (Figure 16E). This study introduces a novel, typical and simple method for directly producing nanostructured materials in just a few minutes, similar to microwave digestion. Except for cobalt vanadate, nickel vanadate has attracted much attention due to the similar electrochemical properties.[153] The chemical kinship (ionic size, electronic structure, etc.) between nickel and cobalt implies that the two vanadate can be synthesized using the versatile methods. For instance, Sambandam et al.[210,211] also reported two MOF-derived $Ni_3V_2O_8$ used as excellent anode material for high-energy lithium-ion batteries.

From the literature discussed above, it can be concluded that polymetallic oxides derived from MOF materials have different morphological characteristics, and the synergistic effect amongst different metals promotes the energy storage capacity and improves the capacity, stability of electrode materials and high electronic conductivity.

5.2.3 | Vanadium phosphate

$M_3V_2(PO_4)_3$ (M = Li or Na) is an excellent cathode material that has attracted much attention in recent years in both lithium-ion batteries and sodium-ion batteries. For instance, $Li_3V_2(PO_4)_3$ (LVP) has high average potential (4.0 V) and specific capacitance (197 mA·h/g), as well as benign ion mobility and excellent thermal stability.[212] Unfortunately, the critical defect of LVP proves its exceedingly poor intrinsic electron transfer efficiency, which severely limits its high rate of charge and discharge and long circulation performance.[213] To improve the electrical conductivity of electrode materials, carbon

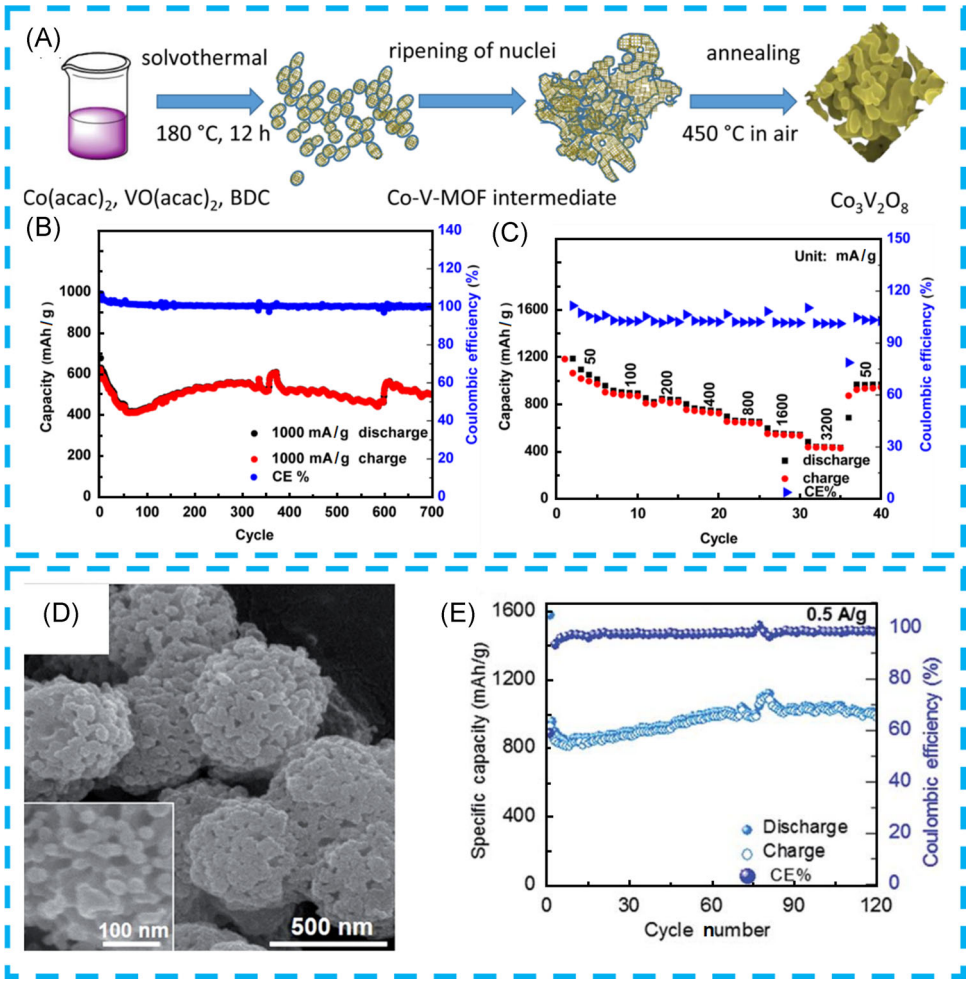

FIGURE 16 (A) Scheme representation of $Co_3V_2O_8$ sponge-like network formation obtained through Co-V-MOF intermediate and Ostwald ripening processes. (B) Cyclability curve for the $Co_3V_2O_8$ at high current density of 1000 mA/g. (C) Rate performance of $Co_3V_2O_8$ at various current densities. Reproduced with permission: Copyright 2016, American Chemical Society.[153] SEM images (D) and corresponding cyclability (E) of $Co_3V_2O_8$. Reproduced with permission: Copyright 2016, Royal Society of Chemistry.[154] SEM, scanning electron microscope

from various sources is widely used in the coating of electrode materials, such as starch, polyvinylidene difluoride (PVDF), glucose, citric acid, and so on.[214] Interestingly, under controlled pyrolysis conditions, MOFs precursors provide significant carbon sources while being used to synthesize LVP.

Wang et al.[184] prepared $Li_3V_2(PO_4)_3$/phosphorus-doped carbon (LVP/P-C) nanocomposites with multilevel structures via one-pot in-situ synthesis using hybrid V-MOFs as precursor. It is worth noting in this study that glass fiber drawing wastewater (GFDW) containing starch, hydroquinone, formaldehyde and various surfactants was used as ligands in the synthesis of hybrid V-MOFs, and the soft templates in GFDW played a role in synthesizing the LVP/P-C nanocomposites with multilevel structures (Figure 17A–C). Compared with LVP and LVP/C, the best performance was achieved by LVP/P-C, leading to a discharge specific capacity of 138 and 65 mA·h/g at 0.1 and 10 C, respectively, and its capacity retention can reach 90% after 1100 cycles (Figure 17D). Most importantly, the waste utilization of GFDW not only improved the performance of lithium-ion batteries, but also alleviated its impact on the environment to a certain extent. MIL-101(V) with molecular formula of $[V_3O(BDC)_3(H_2O)_2Cl_{0.7}(HBDC)_{0.3}]$ ·$2H_2O$·0.5EtOH can also be used as both carbon source and vanadium source to prepare the carbon-coated $Li_3V_2(PO_4)_3$ composite material (LVP/M-101).[151] In Figure 17E,F, it depicts that the as-prepared LVP/M-101 has laminated structures with some hollow bubbles inside and the residual carbon outside. Compared with LVP prepared using V_2O_5, LVP@M-101 electrode exhibited superior behavior at various current densities from 0.1 to 10 C, and the high capacity of 126.6 mA·h/g was recovered when the current density was reversed back to 0.1 C, indicating the stability of the MOFs derived structure (Figure 17G).

Similar to LVP, $Na_3V_2(PO_4)_3$ (NVP) is also considered as a very promising cathode material in SIBs due to its

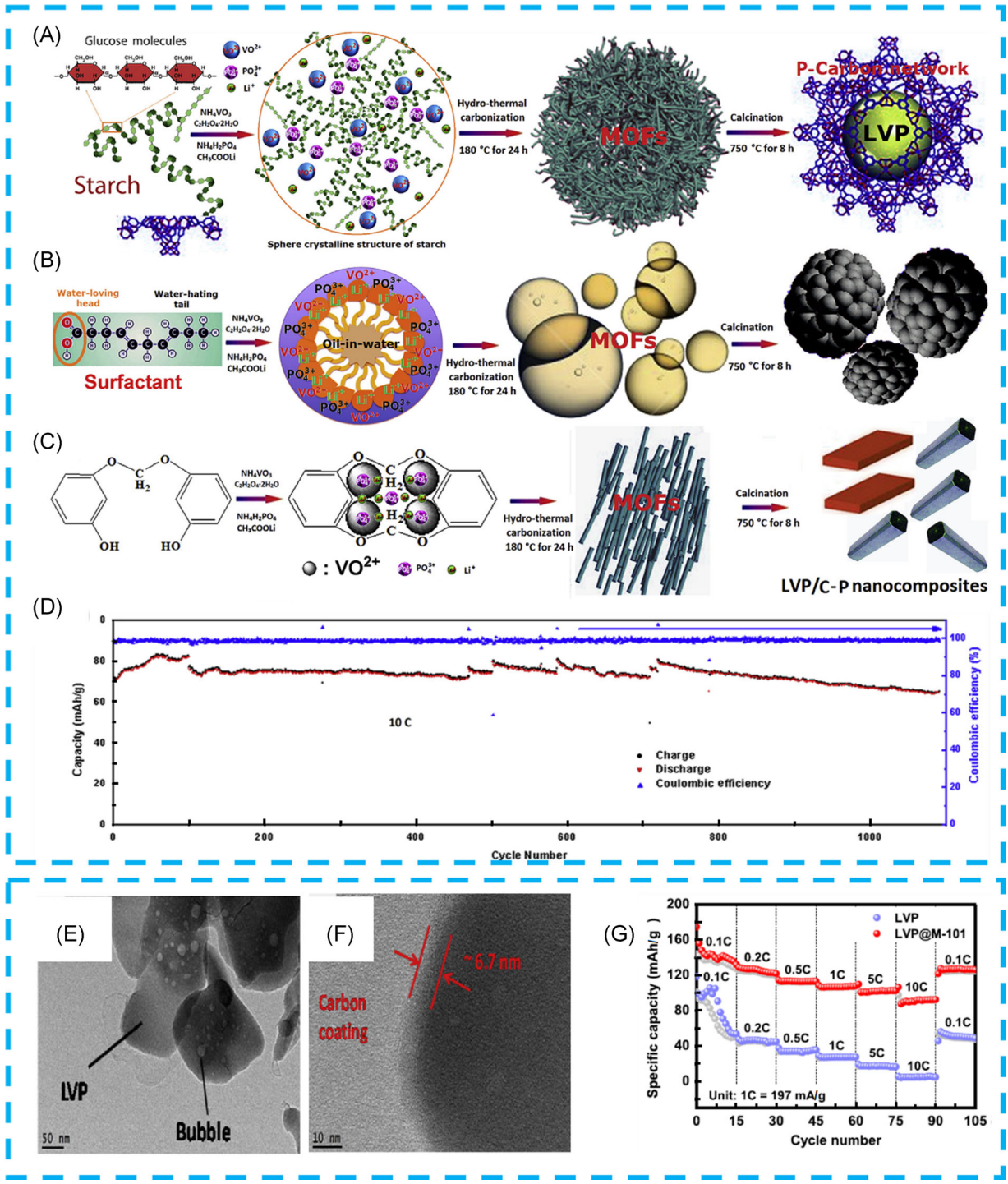

FIGURE 17 Possible synthesis mechanism of the LVP/P-C nanocomposite with different morphologies. Formation schematic diagrams of (A) flower-like structure, (B) spheroidal foam structures and (C) prism structures. (D) Capacity retention and Coulombic efficiency of the LVP/P-C-3 sample for 1100 cycles at 10 C. Reproduced with permission: Copyright 2017, Elsevier B.V.[184] (E-F) TEM images of LVP@M-101. (G) Rate capabilities of LVP@M-101 and LVP electrode at different current densities from 0.1 C to 10 C in the range of 3.0–4.8 V versus Li/Li^+. Reproduced with permission: Copyright 2018, Elsevier B.V.[151]

excellent cycling life and rate performances.[215–217] NVP not only provides an effective space and path for the storage and transport of Na^+ and electrons, but also can effectively restrain the volume change and prevent the agglomeration of electrode materials in the processes of charge and discharge. A new $Na_3V_2(PO_4)_3$ ultrathin sheet/N-doping hard carbon ultrathin sheet (NVPUS/NHCUS) with stable sandwich framework was synthesized by using V-MOFs as

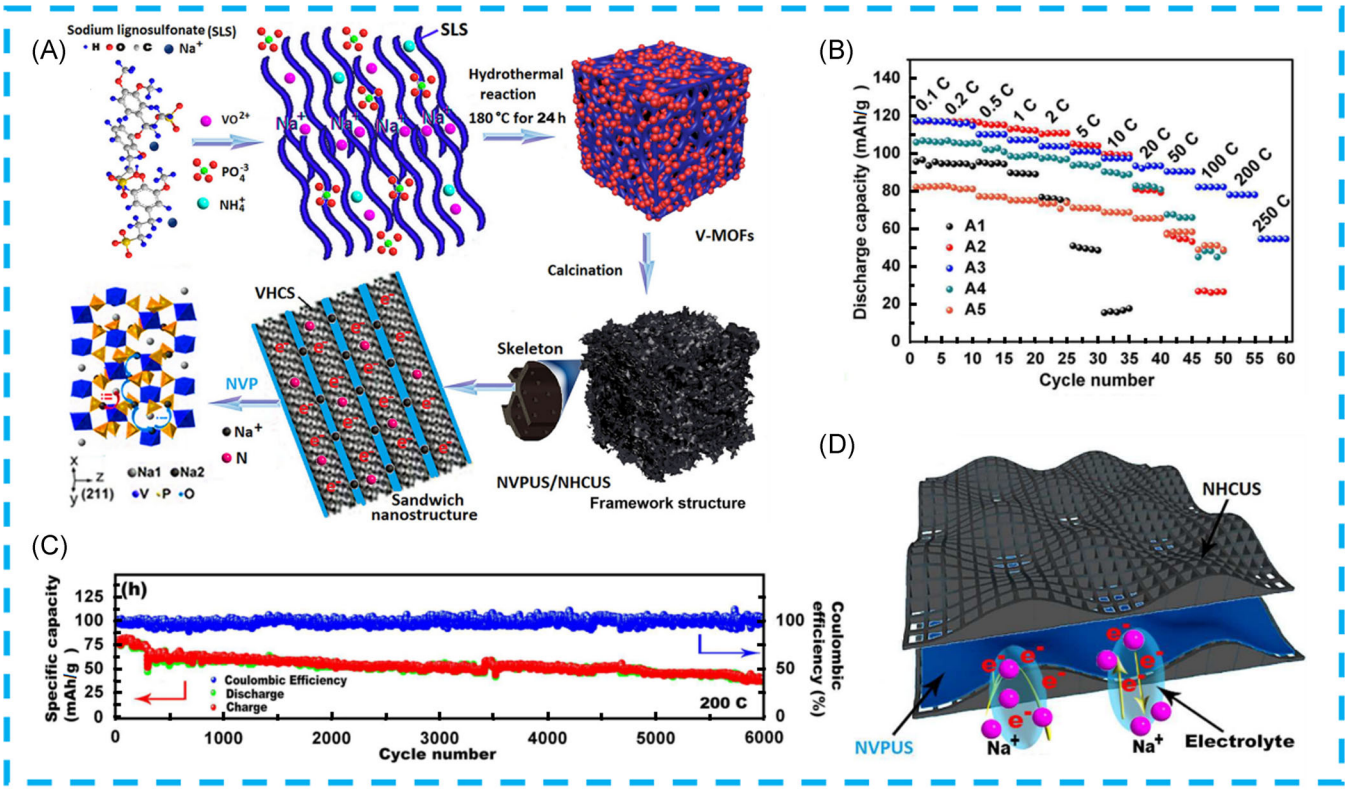

FIGURE 18 (A) Schematic diagram of the synthesis of NVPUS/NHCUS with framework structure derived from polymer sodium lignosulfonate. (B) Rate capabilities of samples from 0.1 to 250 C. (C) Long-term cycling stability and Coulombic efficiency of NVPUS/NHCUS cathode for 6000 cycles at 200 C. (D) Schematic representation exhibiting the high-efficiency electron/Na ion transport pathway for fast sodium insertion. Reproduced with permission: Copyright 2018, Wiley-VCH.[185] NVPUS/NHCUS, $Na_3V_2(PO_4)_3$ ultrathin sheet/N-doping hard carbon ultrathin sheet

precursors, and the multifunctional sodium ligninsulfonate (SLS) was both an organic ligand of V-MOFs and a carbon source (Figure 18A).[185] Thanks to the collective and synergistic effects of electrochemical reactions at the nanoscale, the optimized NVPUS/NHCUS nanocomposite cathode shows the excellent electrochemical property (117.3 mA·h/g at the 0.1 C and remains 40 mA·h/g at 200 C after 6000 cycles) (Figure 18B,C). However, for traditional NVP spheroidal particle it has a relatively poor electron/sodium transport pathway as the phase transition reaction only takes place on the outer surface of the particle. In contrast, the NVPUS/NHCUS shows a highly efficient electron/sodium transport pathway for rapid insertion of sodium ions and provides a large electrode/electrolyte interface area as well (Figure 18D).

6 | CONCLUSIONS AND PERSPECTIVES

In conclusion, this paper reviewed the structural properties and the electrochemical energy conversion and storage applications, including electrocatalysis, supercapacitors and rechargeable batteries, of various V-MOFs and their derivatives. V-MOFs have attracted extensive attention in these fields due to the porous structure and various redox behaviors caused by abundant chemical valences of V-containing nodes. Furthermore, a variety of V-MOF derived materials have also been used as electrocatalysts or electrodes. V-MOFs derivatives with good electrochemical performances can be obtained by choosing the appropriate V-MOFs precursor and controlling the temperature and atmosphere of calcination. During the calcination process, the porous structure and channels are maintained for electrolyte penetration and electron transport by the removal of organic ligands, and the carbon layer formed in situ under an inert atmosphere greatly increased the conductivity and stability of catalyst or electrode material. In addition, the introduction of heteroatoms (O, C, P, etc.) can also provide more active sites, thus improving the electrochemical activity of materials.

Some promising development strategies of V-MOFs and their derivatives for energy conversion and storage applications have also been represented in the following aspects: (1) V-MOFs can be combined with functional materials (graphene, metal nanoparticles, and functional

molecules) to form multifunctional composites with improved electrochemical properties through the synergistic effects; (2) Precise control of MOFs growth can also be used to design and synthesize V-MOFs nanostructures, such as recrystallization, surface-control, and size-confinement; (3) For V-MOFs derivatives, the doping of heteroatoms can be effective to achieve high electrical conductivity and high affinity to adsorb intermediates, and porous carbon skeletons with various doping heteroatoms can be readily obtained by pyrolysis of MOFs with wisely selected organic ligands and encapsulated additives under specific atmosphere such as NH_3, PH_3, and H_2S gases. Although optimistic results have been achieved, research on the application of V-MOFs and its derivatives in energy-related fields deserves further study:

(1) Despite the rich physical and chemical properties of V-MOFs materials, the coordination conditions of vanadium atoms with various organic ligands are relatively strict, which makes periodic V-MOFs materials rarely reported. Therefore, the exploration of V-MOFs that are easier to be prepared will encourage us to develop more vanadium-based materials.
(2) Although various V-MOF derivatives show excellent electrochemical properties, few synthesis strategies have been reported. Thermal treatment is the most widely used preparation method, which is faced with high energy consumption, easy to produce greenhouse gases and harmful gases, structure collapse at high temperature, difficult to accurately control, as well as low yield. Therefore, the green, efficient, and simple strategies of transforming V-MOFs into inorganic nanomaterials are extremely necessary. More importantly, size, morphology and yield of V-MOFs derivatives also need to be precisely controlled.
(3) The open framework and porous structure of MOF have great potential to solve the problems of low capacity or poor cyclic stability of traditional electrode materials when large radius ions (potassium ions) enter the lattice structure. However, as far as the current research results are concerned, there are only a few reports on V-MOFs in potassium ion batteries (PIBs).

Finally, V-MOFs and their derived materials play an increasingly important role in the development of various electrochemical devices. Although some challenges remain, the rapid growth of V-MOFs in recent years has paved the way for the development of more and more novel functional materials for energy conversion and storage.

ACKNOWLEDGMENTS

J. Z., and X. Y. C., contributed equally to this study. The authors gratefully acknowledge the National Natural Science Foundation of China (Nos. 51972067, 22001021, 51802044, 51902062 and 51802043), Guangdong Natural Science Funds for Distinguished Young Scholar (No. 2019B151502039), Natural Science Foundation of Jiangsu Province (No. BK20201048), Natural Science Research Project of Higher Education Institutions in Jiangsu Province (No. 20KJB150008), Singapore MOE AcRF Tier 1 (No. 2020-T1-001-031), the Open Fund of State Key Laboratory of Tea Plant Biology and Utilization (No. SKLTOF20190119), and the National Research Foundation of Singapore (NRF) Investigatorship (No. NRF2016NRF-NRFI001-22).

CONFLICTS OF INTEREST

The authors declare no conflicts of interest.

DATA AVAILABILITY STATEMENT

The data that support the findings of this study are available from the corresponding author upon reasonable request.

ORCID

Qingyu Yan https://orcid.org/0000-0003-0317-3225

REFERENCES

1. Larcher D, Tarascon JM. Towards greener and more sustainable batteries for electrical energy storage. *Nat Chem*. 2015;7(1):19-29.
2. Zhou M, Bai P, Ji X, Yang J, Wang C, Xu Y. Electrolytes and interphases in potassium ion batteries. *Adv Mater*. 2021;33(7):2003741.
3. Dunn B, Kamath H, Tarascon JM. Electrical energy storage for the grid: a battery of choices. *Science*. 2011;334(6058):928-935.
4. Zhao T, Shen X, Wang Y, et al. In situ reconstruction of V-doped Ni_2P pre-catalysts with tunable electronic structures for water oxidation. *Adv Funct Mater*. 2021;31(25):2100614.
5. Zhao C-X, Liu J-N, Wang J, Ren D, Li B-Q, Zhang Q. Recent advances of noble-metal-free bifunctional oxygen reduction and evolution electrocatalysts. *Chem Soc Rev*. 2021;50(13):7745-7778.
6. Menezes PW, Indra A, Das C, et al. Uncovering the nature of active species of nickel phosphide catalysts in high-performance electrochemical overall water splitting. *ACS Catal*. 2017;7(1):103-109.
7. He Y, Guo H, Hwang S, et al. Single cobalt sites dispersed in hierarchically porous nanofiber networks for durable and high-power PGM-free cathodes in fuel cells. *Adv Mater*. 2020;32(46):2003577.
8. Su X, Yang X-F, Huang Y, Liu B, Zhang T. Single-atom catalysis toward efficient CO_2 conversion to CO and formate products. *Acc Chem Res*. 2019;52(3):656-664.
9. Zhao X, Hu G, Chen G-F, Zhang H, Zhang S, Wang H. Comprehensive understanding of the thriving ambient

electrochemical nitrogen reduction reaction. *Adv Mater*. 2021;33(33):2007650.
10. Zhou KL, Han CB, Wang Z, et al. Atomically dispersed platinum modulated by sulfide as an efficient electrocatalyst for hydrogen evolution reaction. *Adv Sci*. 2021;8(12):2100347.
11. Wang K, Du H, He S, et al. Kinetically controlled, scalable synthesis of γ-FeOOH nanosheet arrays on nickel foam toward efficient oxygen evolution: the key role of in-situ-generated γ-NiOOH. *Adv Mater*. 2021;33(11):2005587.
12. Wang J, Li H, Liu S, et al. Turning on Zn 4s electrons in a N_2-Zn-B_2 configuration to stimulate remarkable ORR performance. *Angew Chem Int Ed*. 2021;60(1):181-185.
13. Tang C, Chen L, Li H, et al. Tailoring acidic oxygen reduction selectivity on single-atom catalysts via modification of first and second coordination spheres. *J Am Chem Soc*. 2021;143(20):7819-7827.
14. Liu X, Cui S, Sun Z, Ren Y, Zhang X, Du P. Self-supported copper oxide electrocatalyst for water oxidation at low overpotential and confirmation of its robustness by Cu K-edge X-ray absorption spectroscopy. *J Phys Chem C*. 2016;120(2):831-840.
15. Fan J, Chen Z, Shi H, Zhao G. In situ grown, self-supported iron-cobalt-nickel alloy amorphous oxide nanosheets with low overpotential toward water oxidation. *Chem Commun*. 2016;52(23):4290-4293.
16. Zhou Y, Wang C-H, Lu W, Dai L. Recent advances in fiber-shaped supercapacitors and lithium-ion batteries. *Adv Mater*. 2020;32(5):1902779.
17. Hwang JY, Myung ST, Sun YK. Sodium-ion batteries: present and future. *Chem Soc Rev*. 2017;46(12):3529-3614.
18. Lv CD, Zhou X, Zhong LX, Yan CS, Srinivasan M, Seh ZW, Liu CT, Pan HG, Li SZ, Wen YG, Yan QY. Machine learning: an advanced platform for materials development and state prediction in lithium-ion batteries. *Adv. Mater*. 2021;. http://doi.org/10.1002/adma.202101474.
19. Centi G. Smart catalytic materials for energy transition. *SmartMat*. 2020;1:e1005.
20. Kong L, Tang C, Peng H, Huang J, Zhang Q. Advanced energy materials for flexible batteries in energy storage: a review. *SmartMat*. 2020;1:e1007.
21. Liu T, Zhang L, Cheng B, Yu J. Hollow carbon spheres and their hybrid nanomaterials in electrochemical energy storage. *Adv Energy Mater*. 2019;9(17):1803900.
22. Li B, Lai C, Zhang M, et al. Graphdiyne: a rising star of electrocatalyst support for energy conversion. *Adv Energy Mater*. 2020;10(16):2000177.
23. Nishihara H, Kyotani T. Templated nanocarbons for energy storage. *Adv Mater*. 2012;24(33):4473-4498.
24. Zou L, Hou CC, Wang Q, et al. A honeycomb-like bulk superstructure of carbon nanosheets for electrocatalysis and energy storage. *Angew Chem Int Ed*. 2020;59(44):19627-19632.
25. Wu Q, Yang L, Wang X, Hu Z. Carbon-based nanocages: a new platform for advanced energy storage and conversion. *Adv Mater*. 2020;32(27):1904177.
26. Wu Q, Yang L, Wang X, Hu Z. From carbon-based nanotubes to nanocages for advanced energy conversion and storage. *Acc Chem Res*. 2017;50(2):435-444.
27. Fang Z, Li P, Yu G. Gel electrocatalysts: an emerging material platform for electrochemical energy conversion. *Adv Mater*. 2020;32(39):2003191.
28. Nai J, Lou XW. Hollow structures based on Prussian blue and its analogs for electrochemical energy storage and conversion. *Adv Mater*. 2019;31(38):1706825.
29. Wang J, Wang J, Kong Z, Lv K, Teng C, Zhu Y. Conducting-polymer-based materials for electrochemical energy conversion and storage. *Adv Mater*. 2017;29(45):1703044.
30. Gao M-R, Xu Y-F, Jiang J, Yu S-H. Nanostructured metal chalcogenides: synthesis, modification, and applications in energy conversion and storage devices. *Chem Soc Rev*. 2013;42(7):2986-3017.
31. Yun Q, Li L, Hu Z, Lu Q, Chen B, Zhang H. Layered transition metal dichalcogenide-based nanomaterials for electrochemical energy storage. *Adv Mater*. 2020;32(1):1903826.
32. Li H, Jia X, Zhang Q, Wang X. Metallic transition-metal dichalcogenide nanocatalysts for energy conversion. *Chem*. 2018;4(7):1510-1537.
33. Sun C, Alonso JA, Bian J. Recent advances in perovskite-type oxides for energy conversion and storage applications. *Adv Energy Mater*. 2021;11(2):2000459.
34. Yu XY, Lou XW. Mixed metal sulfides for electrochemical energy storage and conversion. *Adv Energy Mater*. 2018;8(3):1701592.
35. Chen C, Tao L, Du S, et al. Advanced exfoliation strategies for layered double hydroxides and applications in energy conversion and storage. *Adv Funct Mater*. 2020;30(14):1909832.
36. Wang J, Du C-F, Xue Y, et al. MXenes as a versatile platform for reactive surface modification and superior sodium-ion storages. *Exploration*. 2021;1(2):20210024.
37. Li K, Liang M, Wang H, et al. 3D MXene architectures for efficient energy storage and conversion. *Adv Funct Mater*. 2020;30(47):2000842.
38. Yu H, Wang Y, Jing Y, Ma J, Du C-F, Yan Q. Surface modified MXene-based nanocomposites for electrochemical energy conversion and storage. *Small*. 2019;15(25):1901503.
39. Tang J, Huang X, Qiu T, et al. Interlayer space engineering of MXenes for electrochemical energy storage applications. *Chem Eur J*. 2021;27(6):1921-1940.
40. Yang C, Huang H, He H, Yang L, Jiang Q, Li W. Recent advances in MXene-based nanoarchitectures as electrode materials for future energy generation and conversion applications. *Coord Chem Rev*. 2021;435:213806.
41. He T, Kong X-J, Li J-R. Chemically stable metal-organic frameworks: rational construction and application expansion. *Acc Chem Res*. 2021;54(15):3083-3094.
42. Bradshaw D, El-Hankari S, Lupica-Spagnolo L. Supramolecular templating of hierarchically porous metal-organic frameworks. *Chem Soc Rev*. 2014;43(16):5431-5443.
43. Stock N, Biswas S. Synthesis of metal-organic frameworks (MOFs): routes to various MOF topologies, morphologies, and composites. *Chem Rev*. 2012;112(2):933-969.
44. Sindoro M, Yanai N, Jee AY, Granick S. Colloidal-sized metal-organic frameworks: synthesis and applications. *Acc Chem Res*. 2014;47(2):459-469.
45. Li H, Eddaoudi M, O'Keeffe M, Yaghi OM. Design and synthesis of an exceptionally stable and highly porous metal-organic framework. *Nature*. 1999;402(6759):276-279.
46. Mason JA, Veenstra M, Long JR. Evaluating metal-organic frameworks for natural gas storage. *Chem Sci*. 2014;5(1):32-51.
47. Liu J, Chen L, Cui H, Zhang J, Zhang L, Su C-Y. Applications of metal-organic frameworks in heterogeneous

supramolecular catalysis. *Chem Soc Rev*. 2014;43(16):6011-6061.

48. Li JR, Kuppler RJ, Zhou HC. Selective gas adsorption and separation in metal-organic frameworks. *Chem Soc Rev*. 2009;38(5):1477-1504.
49. Garibay SJ, Wang Z, Tanabe KK, Cohen SM. Postsynthetic modification: a versatile approach toward multifunctional metal-organic frameworks. *Inorg Chem*. 2009;48(15):7341-7349.
50. Cohen SM. Postsynthetic methods for the functionalization of metal-organic frameworks. *Chem Rev*. 2012;112(2):970-1000.
51. Xian S, Lin Y, Wang H, Li J. Calcium-based metal-organic frameworks and their potential applications. *Small*. 2021;17(22):2005165.
52. Li B, Wen H, Zhou W, Chen B. Porous metal-organic frameworks for gas storage and separation: what, how, and why? *J Phys Chem Lett*. 2014;5(20):3468-3479.
53. Huang YB, Liang J, Wang XS, Cao R. Multifunctional metal-organic framework catalysts: synergistic catalysis and tandem reactions. *Chem Soc Rev*. 2017;46(1):126-157.
54. Hou CC, Xu Q. Metal-organic frameworks for energy. *Adv Energy Mater*. 2019;9(23):1801307.
55. Liu Z, Zheng F, Xiong W, Li X, Yuan A, Pang H. Strategies to improve electrochemical performances of pristine metal-organic frameworks-based electrodes for lithium/sodium-ion batteries. *SmartMat*. 2021;2(4):488-518.
56. Qiu T, Liang Z, Guo W, Tabassum H, Gao S, Zou R. Metal-organic framework-based materials for energy conversion and storage. *ACS Energy Lett*. 2020;5(2):520-532.
57. Hua Y, Li X, Chen C, Pang H. Cobalt based metal-organic frameworks and their derivatives for electrochemical energy conversion and storage. *Chem Eng J*. 2019;370:37-59.
58. Liang Z, Qu C, Xia D, Zou R, Xu Q. Atomically dispersed metal sites in MOF-based materials for electrocatalytic and photocatalytic energy conversion. *Angew Chem Int Ed*. 2018;57(31):9604-9633.
59. Liang Z, Qu C, Guo W, Zou R, Xu Q. Pristine metal-organic frameworks and their composites for energy storage and conversion. *Adv Mater*. 2018;30(37):1702891.
60. Sanati S, Abazari R, Albero J, et al. Metal-organic framework derived bimetallic materials for electrochemical energy etorage. *Angew Chem Int Ed*. 2021;60(20):11048-11067.
61. Liang Z, Qiu T, Gao S, Zhong R, Zou R. Multi-scale design of metal-organic framework-derived materials for energy electrocatalysis. *Adv Energy Mater*. 2021;121:800. doi:10.1002/aenm.202003410.
62. Indra A, Song T, Paik U. Metal organic framework derived materials: progress and prospects for the energy conversion and storage. *Adv Mater*. 2018;30(39):1705146.
63. Hou CC, Wang HF, Li C, Xu Q. From metal-organic frameworks to single/dual-atom and cluster metal catalysts for energy applications. *Energy Environ Sci*. 2020;13(6):1658-1693.
64. Zou G, Hou H, Ge P, et al. Metal-organic framework-derived materials for sodium energy storage. *Small*. 2018;14(3):1702648.
65. Li W, Kheimeh Sari HM, Li X. Emerging layered metallic vanadium disulfide for rechargeable metal-ion batteries: progress and opportunities. *ChemSusChem*. 2020;13(6):1172-1202.
66. Wan F, Niu Z. Design strategies for vanadium-based aqueous zinc-ion batteries. *Angew Chem Int Ed*. 2019;58(46):16358-16367.
67. Zhang Y, Chen A, Sun J. Promise and challenge of vanadium-based cathodes for aqueous zinc-ion batteries. *J Energy Chem*. 2021;54:655-667.
68. Liu P, Zhu K, Gao Y, Luo H, Lu L. Recent progress in the applications of vanadium-based oxides on energy storage: from low-dimensional nanomaterials synthesis to 3D micro/nano-structures and free-standing electrodes fabrication. *Adv Energy Mater*. 2017;7(23):1700547.
69. Wu C, Feng F, Xie Y. Design of vanadium oxide structures with controllable electrical properties for energy applications. *Chem Soc Rev*. 2013;42(12):5157-5183.
70. Wu C, Xie Y. Promising vanadium oxide and hydroxide nanostructures: from energy storage to energy saving. *Energy Environ Sci*. 2010;3(9):1191-1206.
71. Liu Y-Y, Xu L, Guo X-T, Lv T-T, Pang H. Vanadium sulfide based materials: synthesis, energy storage and conversion. *J Mater Chem A*. 2020;8(40):20781-20802.
72. Yao J, Li Y, Massé RC, Uchaker E, Cao G. Revitalized interest in vanadium pentoxide as cathode material for lithium-ion batteries and beyond. *Energy Storage Mater*. 2018;11:205-259.
73. Liu M, Su B, Tang Y, Jiang X, Yu A. Recent advances in nanostructured vanadium oxides and composites for energy conversion. *Adv Energy Mater*. 2017;7(23):1700885.
74. Van Der Voort P, Leus K, Liu YY, et al. Vanadium metal-organic frameworks: structures and applications. *New J Chem*. 2014;38(5):1853-1867.
75. Li X, Yang X, Xue H, Pang H, Xu Q. Metal-organic frameworks as a platform for clean energy applications. *EnergyChem*. 2020;2(2):100027.
76. Barthelet K, Marrot J, Riou D, Férey G. A breathing hybrid organic-inorganic solid with very large pores and high magnetic characteristics. *Angew Chem Int Ed*. 2002;41(2):281-284.
77. Han X, Hong Y, Ma Y, et al. Adsorption of nitrogen dioxide in a redox-active vanadium metal-organic framework material. *J Am Chem Soc*. 2020;142(36):15235-15239.
78. Liu YY, Couck S, Vandichel M, et al. New VIV-based metal-organic framework having framework flexibility and high CO_2 adsorption capacity. *Inorg Chem*. 2013;52(1):113-120.
79. Leclerc H, Devic T, Devautour-Vinot S, et al. Influence of the oxidation state of the metal center on the flexibility and adsorption properties of a porous metal organic framework: MIL-47(V). *J Phys Chem C*. 2011;115(40):19828-19840.
80. Barthelet K, Marrot J, Férey G, Riou D. $V^{III}(OH)(O_2C–C_6H_4–CO_2)\cdot(HO_2C–C_6H_4–CO_2H)_x(DMF)_y(H_2O)_z$ (or MIL-68), a new vanadocarboxylate with a large pore hybrid topology: reticular synthesis with infinite inorganic building blocks? *Chem Commun*. 2004;4(5):520-521.
81. Barthelet K, Riou D, Férey G. $[V^{III}(H_2O)]_3O(O_2CC_6H_4CO_2)_3\cdot$(Cl, $9H_2O$) (MIL-59): a rare example of vanadocarboxylate with a magnetically frustrated three-dimensional hybrid framework. *Chem Commun*. 2002;14(14):1492-1493.
82. Liu YY, Leus K, Grzywa M, et al. Synthesis, structural characterization, and catalytic performance of a vanadium-based metal-organic framework (COMOC-3). *Eur J Inorg Chem*. 2012;2012(16):2819-2827.
83. Barthelet K, Riou D, Nogues M, Férey G. Synthesis, structure, and magnetic properties of two new vanadocarboxylates with three-dimensional hybrid frameworks. *Inorg Chem*. 2003;42(5):1739-1743.

84. Barthelet K, Adil K, Millange F, Serre C, Rioua D, Férey G. Synthesis, structure determination and magnetic behaviour of the first porous hybrid oxyfluorinated vanado(III)carboxylate: MIL-71 or $V^{III}_2(OH_2F_2(O_2C\text{-}C_6H_4\text{-}CO_2)\cdot H_2O$. *J Mater Chem*. 2003;13(9):2208-2212.
85. Lu Z, Godfrey HGW, Da Silva I, et al. Direct observation of supramolecular binding of light hydrocarbons in vanadium (III) and (IV) metal-organic framework materials. *Chem Sci*. 2018;9(13):3401-3408.
86. Carson F, Su J, Platero-Prats AE, et al. Framework isomerism in vanadium metal-organic frameworks: MIL-88B(V) and MIL-101(V). *Cryst Growth Des*. 2013;13(11):5036-5044.
87. Biswas S, Couck S, Grzywa M, Denayer JFM, Volkmer D, Van der Voort P. Vanadium analogues of nonfunctionalized and amino-functionalized MOFs with MIL-101 topology-synthesis, characterization, and gas sorption properties. *Eur J Inorg Chem*. 2012;15:2481-2486.
88. Breeze MI, Clet G, Campo BC, et al. Isomorphous substitution in a flexible metal-organic framework: mixed-metal, mixed-valent MIL-53 type materials. *Inorg Chem*. 2013;52(14):8171-8182.
89. Lieb A, Leclerc H, Devic T, et al. MIL-100(V)-A mesoporous vanadium metal organic framework with accessible metal sites. *Microporous Mesoporous Mater*. 2012;157:8-23.
90. Vanpoucke DEP. Linker functionalization in MIL-47(V)-R metal-organic frameworks: understanding the electronic structure. *J Phys Chem C*. 2017;121(14):8014-8022.
91. Ghoufi A, Maurin G. Single-file diffusion of neo-pentane confined in the MIL-47(V) metal-organic framework. *J Phys Chem C*. 2019;123(28):17360-17367.
92. Leus K, Couck S, Vandichel M, et al. Synthesis, characterization and sorption properties of NH2-MIL-47. *Phys Chem Chem Phys*. 2012;14(44):15562-15570.
93. Wieme J, Vanduyfhuys L, Rogge SMJ, Waroquier M, Speybroeck VV. Exploring the flexibility of MIL-47(V)-type materials using force field molecular dynamics simulations. *J Phys Chem C*. 2016;120(27):14934-14947.
94. Llewellyn PL, Bourrelly S, Vagner C, et al. Evaluation of MIL-47(V) for CO_2-related applications. *J Phys Chem C*. 2013;117(2):962-970.
95. Alaerts L, Kirschhock CEA, Maes M, et al. Selective adsorption and separation of xylene isomers and ethylbenzene with the microporous vanadium (IV) terephthalate. *Angew Chem Int Ed*. 2007;46(23):4293-4297.
96. Yot PG, Ma Q, Haines J, et al. Large breathing of the MOF MIL-47(V^{IV}) under mechanical pressure: a joint experimental-modelling exploration. *Chem Sci*. 2012;3(4):1100-1104.
97. Yot PG, Wahiduzzaman M, Elkaim E, et al. Modulation of the mechanical energy storage performance of the MIL-47(V^{IV}) metal organic framework by ligand functionalization. *Dalton Trans*. 2019;48(5):1656-1661.
98. Bulánek R, Čičmanec P, Kotera J, Boldog I. Efficient oxidative dehydrogenation of ethanol by VO_x@MIL-101: on par with VO_x/ZrO_2 and much better than MIL-47(V). *Catal Today*. 2019;324:106-114.
99. Kim J, Mcnamara ND, Hicks JC. Catalytic activity and stability of carbon supported V oxides and carbides synthesized via pyrolysis of MIL-47(V). *Applied Catal A: Gen*. 2016;517:141-150.
100. Khan NA, Jun JW, Jeong JH, Jhung SH. Remarkable adsorptive performance of a metal-organic framework, vanadium-benzenedicarboxylate (MIL-47), for benzothiophene. *Chem Commun*. 2011;47(4):1306-1308.
101. Rosenbach N Jr, Jobic H, Ghoufi A, et al. Quasi-elastic neutron scattering and molecular dynamics study of methane diffusion in metal organic frameworks MIL-47(V) and MIL-53(Cr). *Angew Chem Int Ed*. 2008;47(35):6611-6615.
102. Serre C, Millange F, Thouvenot C, et al. Very large breathing effect in the first nanoporous chromium(III)-based solids: MIL-53 or $Cr^{III}(OH)\cdot\{O_2C\text{–}C_6H_4\text{–}CO_2\}\cdot\{HO_2C\text{–}C_6H_4\text{–}CO_2H\}_x\cdot H_2O_y$. *J Am Chem Soc*. 2002;124(45):13519-13526.
103. Urtizberea A, Natividad E, Alonso PJ, et al. Vanadyl spin qubit 2D arrays and their integration on superconducting resonators. *Mater Horizons*. 2020;7(3):885-897.
104. Eddaoudi M, Kim J, Rosi N, et al. Systematic design of pore size and functionality in isoreticular MOFs and their application in methane storage. *Science*. 2002;295(5554):469-472.
105. Biswas S, Vanpoucke DEP, Verstraelen T, et al. New functionalized metal-organic frameworks MIL-47-X (X = –Cl, –Br, $–CH_3$, $–CF_3$, –OH, $–OCH_3$): synthesis, characterization, and CO_2 adsorption properties. *J Phys Chem C*. 2013;117(44):22784-22796.
106. Xu Q, Fang L, Fu Y, Xiao Q, Zhang F, Zhu W. Synthesis, characterization, and CO_2 adsorption properties of metal-organic framework NH_2-MIL-101(V). *Mater Lett*. 2020;264:127402.
107. Abednatanzi S, Derakhshandeh PG, Depauw H. Mixed-metal metal–organic frameworks. *Chem Soc Rev*. 2019;48(9):2535-2565.
108. Masoomi MY, Morsali A, Dhakshinamoorthy A, Garcia H. Mixed-metal MOFs: unique opportunities in metal-organic framework (MOF) functionality and design. *Angew Chem Int Ed*. 2019;58(43):15188-15205.
109. Springuel-Huet MA, Nossov A, Adem Z, et al. 129Xe NMR study of the framework flexibility of the porous hybrid MIL-53(Al). *J Am Chem Soc*. 2010;132(33):11599-11607.
110. Millange F, Serre C, Guillou N, Férey G, Walton RI. Structural effects of solvents on the breathing of metal-organic frameworks: an in situ diffraction study. *Angew Chem Int Ed*. 2008;47(22):4100-4105.
111. Kozachuk O, Meilikhov M, Yusenko K, et al. A solid-solution approach to mixed-metal metal-organic frameworks-detailed characterization of local structures, defects and breathing behaviour of Al/V frameworks. *Eur J Inorg Chem*. 2013;2013(26):4546-4557.
112. Lv J, Liu P, Yang F, et al. 3D hydrangea macrophylla-like nickel-vanadium metal-organic frameworks formed by self-assembly of ultrathin 2D nanosheets for overall water splitting. *ACS Appl Mater Interfaces*. 2020;12(43):48495-48510.
113. Han L, Xu J, Huang Y, Dong W, Jia X. High-performance electrocatalyst of vanadium-iron bimetal organic framework arrays on nickel foam for overall water splitting. *Chin Chem Lett*. 2021;32(7):2263-2268.
114. Rocha J, Almeida Paz FA, Shi FN, Ferreira RAS, Trindade T, Carlos LD. Photoluminescent porous modular lanthanide-vanadium-organic frameworks. *Eur J Inorg Chem*. 2009;2009(33):4931-4945.
115. Tranchemontagne DJ, Tranchemontagne JL, O'keeffe M, Yaghi OM. Secondary building units, nets and bonding in the chemistry of metal-organic frameworks. *Chem Soc Rev*. 2009;38(5):1257-1283.
116. Senchyk GA, Bukhan'ko VO, Lysenko AB, et al. AgI/VV heterobimetallic frameworks generated from novel-type

{$Ag_2(VO_2F_2)_2$(triazole)$_4$} secondary building blocks: a new sspect in the design of SVOF hybrids. *Inorg Chem*. 2012; 51(15):8025-8033.

117. Comito RJ, Wu Z, Zhang G, et al. Stabilized vanadium catalyst for olefin polymerization by site Isolation in a metal-organic framework. *Angew Chem Int Ed*. 2018;57(27):8135-8139.
118. Jaramillo DE, Jiang HZH, Evans HA, et al. Ambient-temperature hydrogen storage via vanadium(II)-dihydrogen complexation in a metal-organic framework. *J Am Chem Soc*. 2021;143(16):6248-6256.
119. Yamabayashi T, Atzori M, Tesi L, et al. Scaling up electronic spin qubits into a three-dimensional metal-organic framework. *J Am Chem Soc*. 2018;140(38):12090-12101.
120. Denysenko D, Werner T, Grzywa M, et al. Reversible gas-phase redox processes catalyzed by Co-exchanged MFU-4l (arge). *Chem Commun*. 2012;48(9):1236-1238.
121. Denysenko D, Jelic J, Reuter K, Volkmer D. Postsynthetic metal and ligand exchange in MFU-4l: a screening approach toward functional metal-organic frameworks comprising single-site active centers. *Chem—A Eur J*. 2015;21(22):8188-8199.
122. Denysenko D, Volkmer D. Cyclic gas-phase heterogeneous process in a metal-organic framework involving a nickel nitrosyl complex. *Faraday Discuss*. 2017;201:101-112.
123. Jaramillo DE, Reed DA, Jiang HZH, et al. Selective nitrogen adsorption via backbonding in a metal-organic framework with exposed vanadium sites. *Nat Mater*. 2020;19(5):517-521.
124. Chen C-L, Goforth AM, Smith MD, Su C-Y, zurLoye H-C. [Co_2(ppca)$_2$(H_2O)(V_4O_{12})$_{0.5}$]: a framework material exhibiting reversible shrinkage and expansion through a single-crystal-to-single-crystal transformation involving a change in the cobalt coordination environment. *Angew Chem Int Ed*. 2005;44(41):6673-6677.
125. Clérac R, Miyasaka H, Yamashita M, Coulon C. Evidence for single-chain magnet behavior in a MnIII-NiII chain designed with high spin magnetic units: a route to high temperature metastable magnets. *J Am Chem Soc*. 2002;124(43):12837-12844.
126. Kitaura R, Onoyama G, Sakamoto H, Matsuda R, Noro S, Kitagawa S. Immobilization of a metallo Schiff base into a microporous coordination polymer. *Angew Chem Int Ed*. 2004;43(20):2684-2687.
127. Bhunia A, Dey S, Moreno JM, et al. A homochiral vanadium-salen based cadmium bpdc MOF with permanent porosity as an asymmetric catalyst in solvent-free cyanosilylation. *Chem Commun*. 2016;52(7):1401-1404.
128. Song F, Wang C, Lin W. A chiral metal-organic framework for sequential asymmetric catalysis. *Chem Commun*. 2011; 47(29):8256-8258.
129. Wu C-D, Hu A, Zhang L, Lin W. A homochiral porous metal-organic framework for highly enantioselective heterogeneous asymmetric catalysis. *J Am Chem Soc*. 2005;127(25):8940-8941.
130. Nguyen HGT, Weston MH, Sarjeant AA, et al. Design, synthesis, characterization, and catalytic properties of a large-pore metal-organic framework possessing single-site vanadyl(mono-catecholate) moieties. *Cryst Growth Des*. 2013;13(8):3528-3534.
131. Goldberg I. Crystal engineering of nanoporous architectures and chiral porphyrin assemblies. *CrystEngComm*. 2008;10(6):637-645.
132. Barron PM, Son HT, Hu C, Choe W. Highly tunable heterometallic frameworks constructed from paddle-wheel units and metalloporphyrins. *Cryst Growth Des*. 2009;9(4):1960-1965.
133. Urtizberea A, Natividad E, Alonso PJ, et al. A porphyrin spin qubit and its 2D framework nanosheets. *Adv Funct Mater*. 2018;28(31):1801695.
134. Long DL, Tsunashima R, Cronin L. Polyoxometalates: building blocks for functional nanoscale systems. *Angew Chem Int Ed*. 2010;49(10):1736-1758.
135. An H, Hou Y, Chang S, Zhang J, Zhu Q. Highly efficient oxidation of various thioethers catalyzed by organic ligand-modified polyoxomolybdates. *Inorg Chem Front*. 2020;7(1):169-176.
136. Kumar D, Landry CC. Immobilization of a Mo, V-polyoxometalate on cationically modified mesoporous silica: synthesis and characterization studies. *Microporous Mesoporous Mater*. 2007;98(1):309-316.
137. Li B, Ma W, Han C, Liu J, Pang X, Gao X. Preparation of MCM-41 incorporated with transition metal substituted polyoxometalate and its catalytic performance in esterification. *Microporous Mesoporous Mater*. 2012;156:73-79.
138. Li Y, Gao Q, Zhang L, et al. $H_5PV_2Mo_{10}O_{40}$ encapsulated in MIL-101(Cr): facile synthesis and characterization of rationally designed composite materials for efficient decontamination of sulfur mustard. *Dalt Trans*. 2018; 47(18):6394-6403.
139. Buru CT, Wasson MC, Farha OK. $H_5PV_2Mo_{10}O_{40}$ polyoxometalate encapsulated in NU-1000 metal-organic framework for aerobic oxidation of a mustard gas simulant. *ACS Appl Nano Mater*. 2020;3(1):658-664.
140. Buru CT, Platero-Prats AE, Chica DG, Kanatzidis MG, Chapman KW, Farha OK. Thermally induced migration of a polyoxometalate within a metal-organic framework and its catalytic effects. *J Mater Chem A*. 2018;6(17):7389-7394.
141. Anjass M, Lowe GA, Streb C. Molecular vanadium oxides for energy conversion and energy storage: current trends and emerging opportunities. *Angew Chem Int Ed*. 2021;60(14): 7522-7532.
142. Dey C, Das R, Poddar P, Banerjee R. Solid phase morphological diversity of a rare vanadium cubane (V_4O_{16}) based metal organic framework. *Cryst Growth Des*. 2012;12(1):12-17.
143. Tian HR, Zhang Z, Liu SM, et al. A novel polyoxovanadate-based Co-MOF: highly efficient and selective oxidation of a mustard gas simulant by two-site synergetic catalysis. *J Mater Chem A*. 2020;8(25):12398-12405.
144. Tian H-R, Zhang Z, Dang T-Y, Liu S-M, Lu Y, Liu S-X. Hollow Lindqvist-like-shaped {V6} cluster-based metal-organic framework for the highly efficient detoxification of mustard gas simulant. *Inorg Chem*. 2021;60(2):840-845.
145. Shen N, Tian F, Chang J, et al. An unprecedented cobalt(ii)-containing Wells-Dawson-type tungstovanadate-based metal-organic framework as an efficient catalyst for ring-opening polymerization of e-caprolactone. *CrystEngComm*. 2020; 22(21):3656-3663.
146. Cai Y, Fang G, Zhou J, et al. Metal-organic framework-derived porous shuttle-like vanadium oxides for sodium-ion battery application. *Nano Res*. 2018;11(1):449-463.
147. Zhang Y, Zou Z, Le S, Li S, Liu J. Effect of heat treatment on structure and properties of cathode materials for V_2O_5 lithium-ion batteries. *J Mater Sci: Mater Electron*. 2020;31(5):3825-3834.
148. Ding Y, Peng Y, Chen W, et al. V-MOF derived porous V_2O_5 nanoplates for high performance aqueous zinc ion battery. *Appl Sur Sci*. 2019;493:368-374.

149. Deng S, Yuan Z, Tie Z, Wang C, Song L, Niu Z. Electrochemically induced metal-organic framework-derived amorphous V_2O_5 for superior rate aqueous zinc-ion batteries. *Angew Chem Int Ed*. 2020;59(49):22002-22006.
150. Kong L, Xie C-C, Gu H, et al. Thermal instability induced oriented 2D pores for enhanced sodium storage. *Small*. 2018; 14(21):1800639.
151. Liao Y, Li C, Lou X, et al. Carbon-coated $Li_3V_2(PO_4)_3$ derived from metal-organic framework as cathode for lithium-ion batteries with high stability. *Electrochimi Acta*. 2018;271:608-616.
152. Soundharrajan V, Sambandam B, Song J, et al. $Co_3V_2O_8$ sponge network morphology derived from metal-organic framework as an excellent lithium storage anode material. *ACS Appl Mater Interfaces*. 2016;8(13):8546-8553.
153. Zhang J, Yuan B, Cui S, et al. Facile synthesis of 3D porous $Co_3V_2O_8$ nanoroses and 2D $NiCo_2V_2O_8$ nanoplates for high performance supercapacitors and their electrocatalytic oxygen evolution reaction properties. *Dalton Trans*. 2017;46(10): 3295-3302.
154. Sambandam B, Soundharrajan V, Mathew V, et al. Metal-organic framework-combustion: a new, cost-effective and one-pot technique to produce a porous $Co_3V_2O_8$ microsphere anode for high energy lithium ion batteries. *J Mater Chem A*. 2016;4(38):14605-14613.
155. Salunkhe RR, Kaneti YV, Yamauchi Y. Metal-organic framework-derived nanoporous metal oxides toward supercapacitor applications: progress and prospects. *ACS Nano*. 2017;11(6):5293-5308.
156. Chen D, Chen C, Baiyee ZM, Shao Z, Ciucci F. Nonstoichiometric oxides as low-cost and highly-efficient oxygen reduction/evolution catalysts for low-temperature electrochemical devices. *Chem Rev*. 2015;115(18):9869-9921.
157. Wei H, Cui D, Ma J, et al. Energy conversion technologies towards self-powered electrochemical energy storage systems: the state of the art and perspectives. *J Mater Chem A*. 2017;5(5):1873-1894.
158. Ye W, Yang Y, Fang X, Arif M, Chen X, Yan D. 2D cocrystallized metal-organic nanosheet array as an efficient and stable bifunctional electrocatalyst for overall water splitting. *ACS Sustain Chem Eng*. 2019;7(21):18085-18092.
159. Wang L, Ren L, Wang X, Feng X, Zhou J, Wang B. Multivariate MOF-templated pomegranate-like Ni/C as efficient bifunctional electrocatalyst for hydrogen evolution and urea oxidation. *ACS Appl Mater Interfaces*. 2018;10(5):4750-4756.
160. Liu M, Zhao Z, Duan X, Huang Y. Nanoscale structure design for high-performance Pt-based ORR catalysts. *Adv Mater*. 2019;31(6):1802234.
161. Yang L, Shui J, Du L, et al. Carbon-based metal-free ORR electrocatalysts for fuel cells: past, present, and future. *Adv Mater*. 2019;31(13):1804799.
162. Hu N, Du J, Ma YY, et al. Unravelling the role of polyoxovanadates in electrocatalytic water oxidation reaction: active species or precursors. *Appl Surf Sci*. 2021;540:148306.
163. Dong W, Zhou H, Mao B, et al. Efficient MOF-derived V-Ni_3S_2 nanosheet arrays for electrocatalytic overall water splitting in alkali. *Int J Hydrogen Energy*. 2021;46(18):10773-10782.
164. Ji Y, Ma Y, Liu R, et al. Modular development of metal oxide/carbon composites for electrochemical energy conversion and storage. *J Mater Chem A*. 2019;7(21):13096-13102.
165. Guo WH, Zhang Q, Wang XH, et al. MOF-derived V-Co_xP@NC nanoarchitectures for highly enhanced electrocatalytic water splitting through electronical tuning. *Electrochim Acta*. 2020;357: 136850.
166. Gopi S, Panda A, Ramu AG, Theerthagiri J, Kim H, Yun K. Bifunctional electrocatalysts for water splitting from a bimetallic (V doped-Ni_xFe_y) metal-organic framework MOF@Graphene oxide composite. *Int J Hydrogen Energy*. 2021. doi:10.1016/j.ijhydene.2021.05.028.
167. Wang Y, Zhang B, Pan W, Ma H, Zhang J. 3D porous nickel-cobalt nitrides supported on nickel foam as efficient electrocatalysts for overall water splitting. *ChemSusChem*. 2017;10(21): 4170-4177.
168. Sun C, Dong Q, Yang J, et al. Metal-organic framework derived $CoSe_2$ nanoparticles anchored on carbon fibers as bifunctional electrocatalysts for efficient overall water splitting. *Nano Res*. 2016;9(8):2234-2243.
169. Raja DS, Chuah X-F, Lu S-Y. In situ grown bimetallic MOF-based composite as highly efficient bifunctional electrocatalyst for overall water splitting with ultrastability at high current densities. *Adv Energy Mater*. 2018;8(23):1801065.
170. Yang D, Chen Y, Su Z, Zhang X, Zhang W, Srinivas K. Organic carboxylate-based MOFs and derivatives for electrocatalytic water oxidation. *Coord Chem Rev*. 2021;428: 213619.
171. Zhou J, Yu L, Zhu Q, Huang C, Yu Y. Defective and ultrathin NiFe-LDH nanosheets decorated on V-doped Ni_3S_2 nanorod arrays: a 3D core-shell electrocatalyst for efficient water oxidation. *J Mater Chem A*. 2019;7(30):18118-18125.
172. Yang D, Cao L, Feng L, et al. Formation of hierarchical Ni_3S_2 nanohorn arrays driven by in-situ generation of VS_4 nanocrystals for boosting alkaline water splitting. *Appl Catal B Environ*. 2019;257:117911.
173. Zhou H, Zheng M, Tang H, Xu B, Tang Y, Pang H. Amorphous intermediate derivative from ZIF-67 and its outstanding electrocatalytic activity. *Small*. 2020;16(2): 1904252.
174. Pan Y, Sun K, Liu S, et al. Core-shell ZIF-8@ZIF-67-derived CoP nanoparticle-embedded N-doped carbon nanotube hollow polyhedron for efficient overall water splitting. *J Am Chem Soc*. 2018;140(7):2610-2618.
175. Zhang J, Chen J, Luo Y, et al. Synergistic coupling of Co_4N/VN confined in N-doped carbon derived from zeolitic imidazolate frameworks for oxygen reduction reaction. *Carbon*. 2020;159:16-24.
176. Muthurasu A, Tiwari AP, Chhetri K, Dahal B, Kim HK. Construction of iron doped cobalt- vanadate- cobalt oxide with metal-organic framework oriented nanoflakes for portable rechargeable zinc-air batteries powered total water splitting. *Nano Energy*. 2021;88:106238.
177. Su G, Chen S, Dong H, et al. Tuning the electronic structure of layered vanadium pentoxide by pre-intercalation of potassium ions for superior room/low temperature aqueous zinc-ion batteries. *Nanoscale*. 2021;13(4):2399-2407.
178. He B, Zhang Q, Man P, et al. Self-sacrificed synthesis of conductive vanadium-based metal-organic framework nanowire-bundle arrays as binder-free cathodes for high-rate and high-energy-density wearable Zn-ion batteries. *Nano Energy*. 2019;64: 103935.

179. Ru Y, Zheng S, Xue H, Pang H. Layered V-MOF nanorods for rechargeable aqueous zinc-ion batteries. *Mater Today Chem*. 2021;21:100513.
180. Hou Y, Mao H, Xu L. MIL-100(V) and MIL-100(V)/rGO with various valence states of vanadium ions as sulfur cathode hosts for lithium-sulfur batteries. *Nano Res*. 2017;10(1):344-353.
181. Lee J-H, Ali G, Kim DH, Chung KY. Metal-organic framework cathodes based on a vanadium hexacyanoferrate Prussian blue analogue for high-performance aqueous rechargeable batteries. *Adv Energy Mater*. 2017;7(2):1601491.
182. Kong L, Zhong M, Liu Y, Xu W, Bu X-H. Ultra-small V_2O_3 embedded N-doped porous carbon nanorods with superior cycle stability for sodium-ion capacitors. *J Power Sources*. 2018;405:37-44.
183. Yang J, Wang B, Jin F, et al. A MIL-47(V) derived hierarchical lasagna-structured V_2O_3@C hollow microcuboid as an efficient sulfur host for high-performance lithium-sulfur batteries. *Nanoscale*. 2020;12(7):4552-4561.
184. Wang Z, He W, Zhang X, et al. Multilevel structures of $Li_3V_2(PO_4)_3$/phosphorus-doped carbon nanocomposites derived from hybrid V-MOFs for long-life and cheap lithium ion battery cathodes. *J Power Sources*. 2017;366:9-17.
185. Yang W, He W, Zhang X, et al. $Na_3V_2(PO_4)_3$/N-doped carbon nanocomposites with sandwich structure for cheap, ultrahigh-rate, and long-life sodium-ion batteries. *ChemElectroChem*. 2019;6(7):2020-2028.
186. Faraji S, Ani FN. The development supercapacitor from activated carbon by electroless plating—a review. *Renew Sustain Energy Rev*. 2015;42:823-834.
187. Abazari R, Sanati S, Morsali A, et al. Ultrafast post-synthetic modification of a pillared cobalt(ii)-based metal-organic framework: via sulfurization of its pores for high-performance supercapacitors. *J Mater Chem A*. 2019;7(19):11953-11966.
188. Zhao R, Liang Z, Gao S, et al. Puffing up energetic metal-organic frameworks to large carbon networks with hierarchical porosity and atomically dispersed metal sites. *Angew Chem Int Ed*. 2019;58(7):1975-1979.
189. Yan Y, Luo Y, Ma J, Li B, Xue H, Pang H. Facile synthesis of vanadium metal-organic frameworks for high-performance supercapacitors. *Small*. 2018;14(33):1801815.
190. Manthiram A, Fu Y, Su Y-S. Challenges and prospects of lithium-sulfur batteries. *Acc Chem Res*. 2013;46(5):1125-1134.
191. Huang J-Q, Zhang Q, Peng HJ, Liu X-Y, Qian W-Z, Wei F. Ionic shield for polysulfides towards highly-stable lithium-sulfur batteries. *Energy Environ Sci*. 2014;7(1):347-353.
192. Yin YX, Xin S, Guo YG, Wan LJ. Lithium-sulfur batteries: electrochemistry, materials, and prospects. *Angew Chem Int Ed*. 2013;52(50):13186-13200.
193. Chen L, Shaw LL. Recent advances in lithium–sulfur batteries. *J Power Sources*. 2014;267:770-783.
194. Zhou J, Li R, Fan X, et al. Rational design of a metal-organic framework host for sulfur storage in fast, long-cycle Li–S batteries. *Energy Environ Sci*. 2014;7(8):2715-2724.
195. Mao Y, Li G, Guo Y, et al. Foldable interpenetrated metal-organic frameworks/carbon nanotubes thin film for lithium–sulfur batteries. *Nat Commun*. 2017;8(1):14628.
196. Bai S, Liu X, Zhu K, Wu S, Zhou H. Metal–organic framework-based separator for lithium–sulfur batteries. *Nat Energy*. 2016;1(7):16094.
197. Neff VD. Some performance characteristics of a Prussian blue battery. *J Electrochem Soc*. 1985;132:1382-1384.
198. You Y, Wu XL, Yin Y-X, Guo Y-G. High-quality Prussian blue crystals as superior cathode materials for room-temperature sodium-ion batteries. *Energy Environ Sci*. 2014;7(5):1643-1647.
199. Huang T, Niu Y, Yang Q, Yang W, Xu M. Self-template synthesis of Prussian blue analogue hollow polyhedrons as superior sodium storage cathodes. *ACS Appl Mater Interfaces*. 2021;13(31):37187-37193.
200. Nagarathinam M, Saravanan K, Phua EJH, Reddy MV, Chowdari BVR, Vittal JJ. Redox-active metal-centered oxalato phosphate open framework cathode materials for lithium ion batteries. *Angew Chem Int Ed*. 2012;51(24):5866-5870.
201. Hameed AS, Reddy MV, Nagarathinam M, et al. Room temperature large-scale synthesis of layered frameworks as low-cost 4V cathode materials for lithium-ion batteries. *Sci Rep*. 2015;5(1):16270.
202. Liao J, Hu Q, Mu J, He X, Wang S, Chen C. A vanadium-based metal-organic phosphate framework material $K_2[(VO)_2(HPO_4)_2(C_2O_4)]$ as a cathode for potassium-ion batteries. *Chem Commun*. 2019;55(5):659-662.
203. Li X, Zheng S, Jin L, et al. Metal-organic framework-derived carbons for battery applications. *Adv Energy Mater*. 2018;8(23):1800716.
204. Ding Y, Peng Y, Chen S, et al. Hierarchical porous metallic V_2O_3@C for advanced aqueous zinc-ion batteries. *ACS Appl Mater Interfaces*. 2019;11(47):44109-44117.
205. Shi R, Wang Y, Zhou F, Zhu R. $Zn_3V_2O_7(OH)_2(H_2O)_2$ and $Zn_3V_2O_8$ nanostructures: controlled fabrication and photocatalytic performance. *J Mater Chem*. 2011;21(17):6313-6320.
206. Luo L, Zeng Y, Li L, Luo Z, Smirnova TI, Maggard PA. Manganese-vanadate hybrids: impact of organic ligands on their structures, thermal stabilities, optical properties, and photocatalytic activities. *Inorg Chem*. 2015;54(15):7388-7401.
207. Mondal C, Ganguly M, Sinha AK, Pal J, Sahoo R, Pal T. Robust cubooctahedron $Zn_3V_2O_8$ in gram quantity: a material for photocatalytic dye degradation in water. *CrystEngComm*. 2013;15(34):6745-6751.
208. Wu M, Yang J, Feng T, et al. Graphene coated $Co_3V_2O_8$ micro-pencils for enhanced-performance in lithium-ion batteries. *New J Chem*. 2017;41(19):10634-10639.
209. Song Y, Liu TY, Yao B, et al. Amorphous mixed-valence vanadium oxide/exfoliated carbon cloth structure shows a record high cycling stability. *Small*. 2017;13(16):1700067.
210. Soundharrajan V, Sambandam B, Song J, et al. Bitter gourd-shaped $Ni_3V_2O_8$ anode developed by a one-pot metal-organic framework-combustion technique for advanced Li-ion batteries. *Ceram Int*. 2017;43(16):13224-13232.
211. Sambandam B, Soundharrajan V, Song J, et al. $Ni_3V_2O_8$ nanoparticles as an excellent anode material for high-energy lithium-ion batteries. *J Electroanal Chem*. 2018;810:34-40.
212. Barker J, Saidi MY, Swoyer JL. A carbothermal reduction method for the preparation of electroactive materials for lithium-ion applications. *J Electrochem Soc*. 2003;150(6):A684-A688.
213. Yin S-C, Strobel PS, Grondey H, Nazar LF. $Li_{2.5}V_2(PO_4)_3$: a room-temperature analogue to the fast-ion conducting high-temperature γ-phase of $Li_3V_2(PO_4)_3$. *Chem Mater*. 2004;16(8):1456-1465.

214. Rui X, Li C, Chen CH. Synthesis and characterization of carbon-coated $Li_3V_2(PO_4)_3$ cathode materials with different carbon sources. *Electrochim Acta*. 2009;54(12):3374-3380.
215. Rui X, Sun W, Wu C, Yu Y, Yan Q. An advanced sodium-ion battery composed of carbon coated $Na_3V_2(PO_4)_3$ in a porous graphene network. *Adv Mater*. 2015;27(42):6670-6676.
216. Wang Q, Zhao B, Zhang S, Gao X, Deng C. Superior sodium intercalation of honeycomb-structured hierarchical porous $Na_3V_2(PO_4)_3$/C microballs prepared by a facile one-pot synthesis. *J Mater Chem A*. 2015;3(15):7732-7740.
217. Xu Y, Wei Q, Xu C, et al. Layer-by-layer $Na_3V_2(PO_4)_3$ embedded in reduced graphene oxide as superior rate and ultralong-life sodium-ion battery cathode. *Adv Energy Mater*. 2016;6(14):1600389.

AUTHOR BIOGRAPHIES

Fei-Long Li is currently an associate professor at Changshu Institute of Technology. He graduated with a BS in chemistry from Soochow University in 2014, and obtained his PhD in inorganic chemistry from Soochow University in 2019. His research interests mainly focus on the design and synthesis of MOFs materials and their applications in electrochemistry.

Xianhong Rui is a professor at Guangdong University of Technology, China. He received his B.S. degree from the University of Jinan in 2007 and his M.S. degree from the University of Science and Technology of China in 2010. He then obtained his Ph.D. degree from the School of Materials Science and Engineering at Nanyang Technological University in 2014. His research interests mainly focus on the design and fabrication of advanced electrode materials for energy conversion and storage.

Qingyu Yan is currently a professor in School of Materials Science and Engineering at Nanyang Technology University. He joined the School of Materials Science and Engineering of Nanyang Technological University as an assistant professor in 2008 and became a professor in 2018. He is currently the chair of the Electrochemical Society, Singapore Section. He is a fellow of the Royal Society of Chemistry since 2018. His research interests focus on nanostructured materials and their integration/assembly for electrode materials for energy-storage devices, thermoelectric modules, magnetic devices, and photovoltaic-module applications.

How to cite this article: Zhu J, Chen X, Thang AQ, et al. Vanadium-based metal-organic frameworks and their derivatives for electrochemical energy conversion and storage. *SmartMat*. 2022;3:384-416. doi:10.1002/smm2.1091